Journal of Controlled Release 372 (2024) 751–777

Contents lists available at ScienceDirect

Journal of Controlled Release

journal homepage: www.elsevier.com/locate/jconrel

Review article

Nanoparticle-mediated thermal Cancer therapies: Strategies to improve clinical translatability

M. Bravo [a,b], B. Fortuni [b], P. Mulvaney [a], J. Hofkens [b,d], H. Uji-i [b,c], S. Rocha [b,*], J. A. Hutchison [a,*]

[a] ARC Centre of Excellence in Exciton Science, School of Chemistry, University of Melbourne, Parkville, VIC 3010, Australia
[b] Molecular Imaging and Photonics, Chemistry Department, KU Leuven, Celestijnenlaan 200F, 3001 Heverlee, Belgium
[c] Research Institute for Electronic Science (RIES), Hokkaido University, N20W10, Kita ward, Sapporo 001-0020, Hokkaido, Japan
[d] Max Planck Institute for Polymer Research, Mainz D-55128, Germany

ARTICLE INFO

Keywords:
Nanomaterials
Photothermal therapy
Magnetothermal therapy
Nanothermometry
3D tumor models

ABSTRACT

Despite significant advances, cancer remains a leading global cause of death. Current therapies often fail due to incomplete tumor removal and nonspecific targeting, spurring interest in alternative treatments. Hyperthermia, which uses elevated temperatures to kill cancer cells or boost their sensitivity to radio/chemotherapy, has emerged as a promising alternative. Recent advancements employ nanoparticles (NPs) as heat mediators for selective cancer cell destruction, minimizing damage to healthy tissues. This approach, known as NP hyperthermia, falls into two categories: photothermal therapies (PTT) and magnetothermal therapies (MTT). PTT utilizes NPs that convert light to heat, while MTT uses magnetic NPs activated by alternating magnetic fields (AMF), both achieving localized tumor damage. These methods offer advantages like precise targeting, minimal invasiveness, and reduced systemic toxicity. However, the efficacy of NP hyperthermia depends on many factors, in particular, the NP properties, the tumor microenvironment (TME), and TME-NP interactions. Optimizing this treatment requires accurate heat monitoring strategies, such as nanothermometry and biologically relevant screening models that can better mimic the physiological features of the tumor in the human body. This review explores the state-of-the-art in NP-mediated cancer hyperthermia, discussing available nanomaterials, their strengths and weaknesses, characterization methods, and future directions. Our particular focus lies in preclinical NP screening techniques, providing an updated perspective on their efficacy and relevance in the journey towards clinical trials.

1. Introduction

Cancer remains a leading cause of mortality worldwide and manifests as a result of genetic mutations that drive uncontrolled cellular growth and spread, a process known as carcinogenesis [1,2]. Cancer cells possess various characteristics that make the disease difficult to cure, including metastatic capabilities, sustained proliferation, cell death resistance, and angiogenesis induction at the tumor site [3]. Traditional mainstays of cancer treatment—chemotherapy, radiation therapy, and surgery—often suffer from limitations such as lack of efficacy and off-target toxicity. This has fueled a growing interest in novel therapeutic alternatives [4]. Heat has been explored as a form of tumor therapy since ancient times, due to the heightened sensitivity of cancer cells to elevated temperatures [5]. However, this strategy has often proven insufficient as a standalone curative modality, due to its low specificity and anti-tumor efficacy [6]. Recently, there has been a renewed interest in exploring hyperthermia (HT) as a solution for improved cancer therapies, motivated by the design of functional nanomaterials with hyperthermal potential [7,8].

In cancer research, HT is used to induce heat shock responses in cancer cells [9]. It is categorized as mild hyperthermia (40–42 °C), moderate hyperthermia (42–45 °C), and thermal ablation (≥ 45 °C) [10]. Mild to moderate HT induces reversible changes in tissue physiology, which depend on the temperature and duration of the treatment (thermal dose). In clinical applications, the common target temperature of 43 °C for up to 1 h is widely accepted, and the thermal dose is commonly expressed as the cumulative equivalent minutes at 43 °C (CEM43) [5]. Changes induced by mild/moderate hyperthermia include

* Corresponding authors.
E-mail addresses: susana.rocha@kuleuven.be (S. Rocha), james.hutchison@unimelb.edu.au (J.A. Hutchison).

https://doi.org/10.1016/j.jconrel.2024.06.055
Received 29 March 2024; Received in revised form 14 June 2024; Accepted 21 June 2024
Available online 4 July 2024

increased blood flow and reoxygenation, altered protein structure, modified metabolic pathways, triggered antitumor immune responses, and inhibited DNA repair mechanisms [5,9,11–13]. Enhanced oxygenation at the tumor site promotes the anti-tumor efficacy of radiotherapy, due to increased production of toxic reactive oxygen species [14]. HT acts as a chemosensitizer, as a result of improved drug accumulation and toxicity promoted by increased blood flow and inhibited DNA repair pathways [15,16]. Lastly, temperature-induced immune response activation acts as a catalyst for anti-tumor immunotherapies [17]. Therefore, HT can enhance cell susceptibility to damage and improve treatment outcomes when used as an adjuvant therapy [5]. When temperatures exceed 45 °C, HT results in irreversible cell damage and tumor destruction. Thermal ablation is often applied for a few minutes, causing coagulation and protein denaturation with consequent cell death, primarily through necrotic mechanisms. Therefore, thermal ablation shows potential for use as a standalone therapeutic approach (Fig. 1) [4,9,13]. Depending on the area of application, HT can be further classified as local, regional, and whole-body treatments. Local HT is usually achieved using radiofrequency (RF), microwave (MW), and ultrasound, conveyed using applicators for the treatment of small tumors, located close to the body surface or within a body cavity [10]. In regional HT treatments, part of the patient's blood is removed, heated, and pumped back into the body to increase the temperature of a body part, such as a limb or a cavity [10]. Lastly, in whole-body HT, the temperature of the human body is raised to 43 °C *via* thermal baths [18]. While numerous studies have elucidated the temperature-dependent effects on different cancer types, HT faces challenges such as heterogeneous tumor heating, off-target toxicity, and limited overall efficacy [12]. To address these issues, researchers have turned to the development of nanoparticles (NPs) that passively accumulate at the tumor site and can generate heat upon external stimuli. Their use can enhance treatment specificity by locally generating heat at the tumor, maximizing the energy deposited in the cancer cells while minimizing exposure in healthy cells [19].

Nanotechnology has revolutionized cancer therapy due to the unique properties of nanoscale materials. NPs can be designed in a panoply of different sizes and shapes, exhibit high biocompatibility, and can display efficient cellular targeting, with rapid adhesion and endocytosis, intracellular trafficking, and easy bioelimination/biodegradation [20]. Typically, NPs for cancer treatment range in size between 20 and 200 nm, allowing for increased blood circulation times and easy uptake by the cells [21–23]. Due to their small size, it is widely accepted that these NPs can passively extravasate the leaky tumor vasculature and preferentially accumulate in tumors *via* the enhanced permeability and retention (EPR) effect [24]. NP specificity can be further enhanced following surface modification for active cancer cell targeting, through the conjugation of ligands that bind specifically to tumor biomarkers [25,26]. This tumor-specific NP accumulation allows for higher therapeutic specificity and a lower probability of off-target toxicity to healthy cells [13].

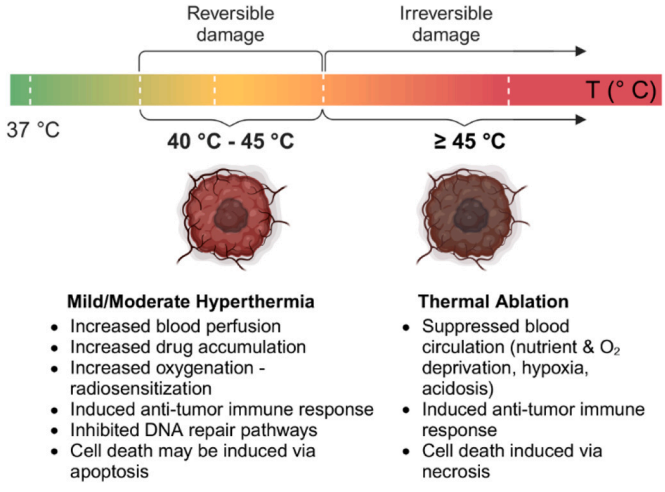

Fig. 1|. Temperature-dependent effects of hyperthermia in cancer treatment. Cancer thermal therapies can be classified based on the desired temperature and induced cell damage. At lower temperatures (below 45 °C), cell damage is reversible and often leads to increased chemo- and radiosensitivity, making for an interesting adjuvant strategy to conventional therapeutic approaches. Above 45 °C, the damage becomes irreversible, and cell death is induced *via* necrosis. This strategy is known as thermal ablation and has shown potential as a monotherapy. (Image created with BioRender.com).

Over the past decades, numerous multi-functional nanomaterials have been developed as novel cancer therapeutics. The FDA (U.S. Food and Drug Administration) approved the first NP-based cancer therapy in 1995, which consisted of a liposome as a carrier for the chemotherapy agent Doxorubicin® [27]. Since then, various materials have been approved for clinical use, with the majority being nanoscale carriers for chemotherapeutic drugs (Table 1) [28]. To date, only one formulation has been approved for NP-mediated cancer-therapies (NanoTherm®), but several clinical trials are currently underway.

This review complements previous comprehensive reports on the wide range of NPs available for NP-HT [29–31,42], yet it will further explore novel temperature monitoring techniques, which are crucial for ensuring precise and controlled thermal effects during treatment. Furthermore, we extend this overview to advanced 3D *in vitro* cell models that closely replicate the intricacies of the biological environment, providing a more realistic assessment of NP behavior. By highlighting these emerging areas, this review aims to contribute to the current discourse and provide a timely and relevant resource for researchers in the field.

2. The potential of nanoparticles in hyperthermia

In NP-HT, cell death is induced by local heat generation upon NP activation. Once NPs are accumulated in the tumor tissue, activation occurs *via* remote external stimuli [18,43]. As a result, NPs can promote tumor-restrained temperature increases *via* an inside-out strategy (Fig. 2). This presents a considerable advantage compared to conventional HT therapies, which often create a temperature gradient that decreases with distance from the heat source (outside-in strategies). The outside-in temperature gradient increases the chance of toxicity to healthy cells while impairing therapeutic efficacy at the tumor site [4,13]. Remote NP activation can be achieved *via* laser light irradiation, RF waves, alternating magnetic field (AMF), or ultrasound waves [18,43]. Laser irradiation and AMF activation, commonly known as photothermal therapies (PTT) and magnetothermal therapies (MTT), respectively, are the most reported strategies. While PTT harnesses the unique properties of NPs that can absorb light and convert it into localized heat, MTT employs NPs that generate heat in response to rapidly alternating external magnetic fields [8].

The following section presents an updated review of the different types of nanomaterials currently studied for MTT and PTT, as well as the primary heat generation mechanisms and main advantages and disadvantages of each strategy in cancer therapeutics.

2.1. NP-mediated Magnetothermal therapies

MTT, also referred to as magnetic fluid hyperthermia, is a minimally invasive technique that allows for deep tissue heating. It occurs when magnetic NPs (MNPs) generate heat *via* magnetic energy loss upon exposure to an external magnetic field. The temperature increase leads to cell death and consequent tumor destruction [44]. The potential of MNPs in HT was first demonstrated in 1957 by Gilchrist et al., who used AMF to activate iron oxide NPs and increase the temperature of lymph nodes [45]. Since then, numerous strategies have been developed to improve the performance of MNPs in cancer therapeutics [44,46,47]. Recently, the work of Jordan et al. culminated in the European

Table 1|
List of approved nanomedicines for cancer treatment, ordered by year of first approval.

Tradename	Material	Therapeutic agent	Indication	Year of Approval	Reference
Doxil®/ Caelyx®	PEGylated liposome	Doxorubicin	Breast cancer Ovarian cancer Kaposi's sarcoma Multiple myeloma	1995 (FDA), 1996 (EMA)	[27]
DaunoXome®	Liposome	Daunorubicin	Kaposi's sarcoma	1996 (FDA)	[32]
DepoCyt®	Liposome	Cyratabine	Neoplastic meningitis	1999 (FDA), 2001 (EMA)	[28,33]
Myocet Liposomal®	Liposome	Doxorubicin	Metastatic breast cancer	2000 (EMA)	[28,34]
Eligard®	PLGA	Paclitaxel	Prostate cancer	2004 (FDA)	[35]
Abraxane®	Albumin NP	Paclitaxel	Breast cancer Lung cancer Pancreatic cancer	2005 (FDA), 2008 (EMA)	[36]
Genexol-PM®	Polymeric micelle	Paclitaxel	Breast cancer Lung cancer	2007 (Korea)	[28]
Oncaspar®	Polymer protein conjugate	L-asparaginase	Acute lymphoblastic leukemia	2006 (FDA), 2016 (EMA)	[37]
Mepact®	Liposome	Mifamurtide	Osteosarcoma	2009 (EMA)	[38]
NanoTherm®	Iron oxide NP (Fe_2O_3)	Heat	Glioblastoma	2010 (EMA)	[28,39]
Marqibo®	Liposome	Mifamurtide	Acute lymphoid leukemia	2012 (FDA)	[40]
Onivyde®	Liposome	Irinotecan	Pancreatic cancer	2015 (FDA)	[40]
Vyxeos®	Liposome	Cytarabine/Daunorubicin	Acute myeloid leukemia	2017 (FDA)	[41]
Hensify®	Hafnium oxide NP	Ionizing radiation	Soft tissue Sarcoma	2019 (EMA)	[41]

Abbreviations: PEG – Polyethylene glycol; FDA – U.S. Food and Drug Administration; EMA – European Medicines Agency; PLGA - Poly(lactic-*co*-glycolic acid).

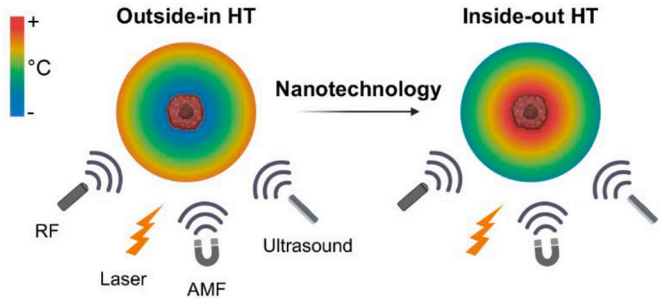

Fig. 2|. Schematic representation of conventional outside-in *vs.* inside-out HT therapies, promoted by NP-HT. When accumulated at the tumor site, NPs can generate localized heat in response to external energy sources. (Image created with BioRender.com).

Medicines Agency's (EMA) approval of aminosilane-coated superparamagnetic iron oxide NPs (SPIONs) for the clinical treatment of glioblastoma multiforme (NanoTherm®, see Table 1) [48].

2.1.1. Magnetism - heat generation mechanisms

At the nanoscale, local heat generation by MNPs can be attributed to hysteresis losses and/or relaxation losses (Néel and Brownian relaxations) (Fig. 3) [49]. The dominant heating mechanism is determined by structural NP properties such as size, shape, composition, and magnetization, as well as environmental parameters, including viscosity and temperature [44,50]. Magnetic materials have magnetic moments or dipoles with direction and magnitude that depend on their chemical and crystalline structure. Ferromagnetic/ferrimagnetic materials present multi-magnetic domains (Weiss domains) that consist of a series of aligned magnetic moments or dipoles. When subjected to cyclic magnetization changes, these magnetic domains are forced to adjust their orientation to align with the external magnetic field, reaching saturation magnetization. The motion of domain walls is responsible for energy dissipation in the form of heat. These energy losses are known as hysteresis losses and are the primary heat generation mechanism in multi-domain MNPs (Fig. 3a) [51]. This behavior can be represented by hysteresis loops, which plot the relationship between the strength of the applied magnetic field (H) and the resulting magnetization of the material (M) (Fig. 3b, d). Hysteresis loops can be measured by superconducting quantum interference device (SQUID) measurements, which can detect MNP stability in terms of magnetometry at different temperatures [52]. In these plots, it is possible to estimate the coercivity of the material, *i.e.* the resistance of the MNP to changes in magnetization. Multi-domain NPs often show higher resistance to magnetization changes when an external AMF is applied (higher coercivity), leading to residual magnetism that is only overcome by applying a coercive force. This results in energy dissipation from the system, which is proportional to the area of the hysteresis loop [53]. Single-domain MNPs, particularly superparamagnetic materials, show no resistance to magnetization variations and, therefore, zero coercivity (Fig. 3d) [53]. In superparamagnetic NPs, there is no heat generation *via* hysteresis losses, and temperature increases occur mainly due to Brownian-Néel relaxation phenomena (Fig. 3c). Néel relaxation results from the rapid flip of internal magnetic moments between two stable orientations separated by an energy barrier. Brownian relaxation mechanisms occur due to the physical rotation of the whole MNP suspended in a viscous fluid. Relaxation losses are generally accepted as the dominant heat generation mechanism for smaller MNPs ($\geq$ 50–20 nm, depending on the material) [6,44,54,55]. A more detailed explanation of the mechanisms behind heat generation by MNPs can be found elsewhere, for example, two excellent review papers by Das et al. [44], and by Mody et al. [53].

The ablative efficiency of MTT is determined by the specific absorption rate (SAR) or specific loss power (SLP) of the nanomaterial, which quantifies the amount of heat released per unit of time, per unitary amount of active material [57]. The SAR is dependent on the parameters of the applied AMF (amplitude and frequency), the properties of the NPs (*e.g.*, size, shape, composition, and surface functionalization), and the administered concentration of MNPs [44]. For this reason, in the clinic, these parameters need to be finely tuned to ensure optimized MNP activation with minimal off-target heating of healthy tissues [6]. While AMF induces heat generation by MNPs due to the generation of a magnetic field, it can also generate an electric field. This electric field penetrates biological tissue and induces eddy currents that lead to unintentional tissue heating [58]. Therefore, it is generally accepted that the AMF parameters should be limited to amplitudes between 5 and 20 $kA{\cdot}m^{-1}$ and frequencies below 1 MHz. In the 1980s, Atkinson et al., and later Brezovich et al., studied the effect of AMF on humans and found that the product of AMF frequency and amplitude ($H \times f$) must be kept under 4.85×10^8 Am^{-1} s^{-1}. This is currently known as the Atkinson-Brezovich safety limit [59–61]. Recently, different studies have

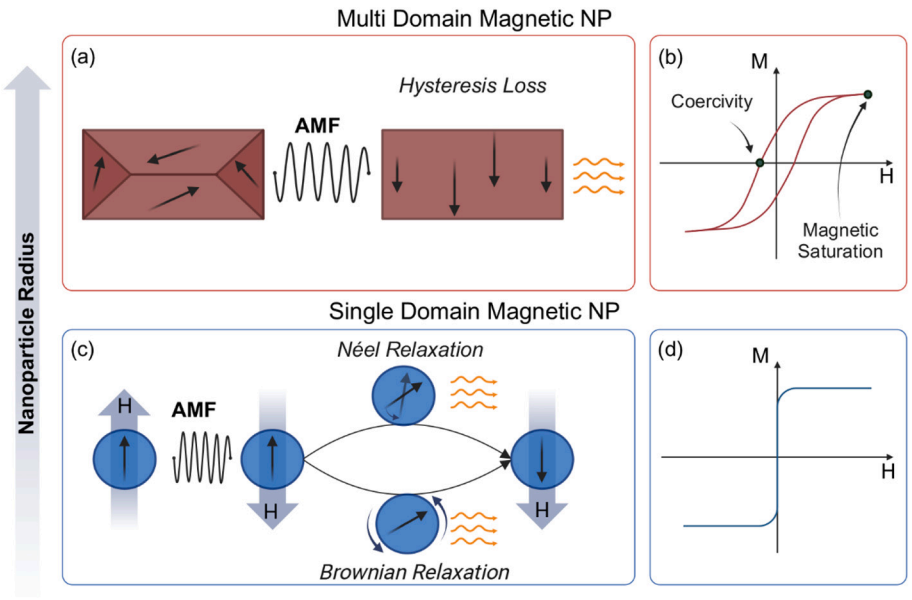

Fig. 3|. Schematic representation of heat generation mechanisms in MNPs. (a) Larger multi-domain MNPs typically generate heat due to hysteresis losses as a consequence of the motion of the domain walls; (b) Typical hysteresis loop obtained for multi-domain MNPs; (c) Single-domain MNPs can undergo Brownian and/or Néel relaxation. In Brownian relaxation mechanisms, the entire particle rotates within the fluid, generating energy losses. Néel relaxation processes are related to the rotation of the magnetic moment within the MNP core; (d) Typical hysteresis loop obtained for superparamagnetic MNPs. M is the magnetization of the material, and H is the applied magnetic field intensity Adapted from [53,56]. (Image created with BioRender.com).

proposed revising the magnetic safety limit up to 5×10^9 Am^{-1} s^{-1}, one order of magnitude higher than the Atkinson-Brezovich limit [62]. In fact, the clinically approved NanoTherm® formulation, administered to glioblastoma patients, is activated using magnetic fields up to 1.8×10^9 Am^{-1} s^{-1} (18kA/m at 100 kHz) [62].

2.1.2. *Magnetic nanoparticles: The advantage of Iron oxide*

Due to their size-dependent magnetic properties and biocompatibility, MNPs have potential applications in hyperthermia, controlled drug release, magnetic resonance imaging (MRI) and biosensing [47]. For this reason, numerous methods have been described to synthesize and modify MNPs, and several examples of highly efficient, targeted NPs for cancer MTT have been reported [44,46]. Over the past decades, several studies have been performed to improve NP-MTT. A panoply of nanoformulations has been described both *in vitro* and *in vivo*, aiming to enhance SAR values (examples listed in Table 2). Some of the available MNPs include metal NPs [*e.g.* iron (Fe), cobalt (Co), nickel (Ni) and gadolinium (Gd)], metal oxide NPs, metal alloy NPs, and core-shell magnetic NPs.

From these different MNPs, iron oxide NPs (IONPs) are the most widely investigated materials in NP-MTT [63]. In addition to their high biocompatibility and FDA approval, iron oxide shows lower susceptibility to oxidation than other MNPs. Furthermore, IONP synthesis is versatile and yields a wide range of sizes [42,64]. IONPs can be classified as hematite (α-Fe_2O_3), maghemite (γ-Fe_2O_3), and magnetite (α-Fe_3O_4). Among these, magnetite displays an ideal magnetic moment and has been the most commonly studied formulation for thermal ablation applications [42]. While bulk iron oxide consists of a ferrimagnetic multi-domain magnet, below a critical diameter (≈ 30 nm), IONPs behave as single-domain NPs, commonly known as SPIONs (superparamagnetic iron oxide NPs). As explained in the previous section, SPIONs have zero coercivity and high magnetic susceptibility. They can quickly flip their magnetic dipole orientation in the presence of an AMF and generate heat *via* Néel-Brownian relaxation processes [63,65]. Compared to ferrimagnetic IONPs, SPIONs are generally preferred for biomedical applications as they often require lower AMF intensities for high SAR values. In addition, SPIONs display zero magnetization in the absence of an external AMF, which significantly decreases aggregation [66]. Despite their tremendous potential, SPIONs are often stable in organic solvents and incompatible with an aqueous environment, and their thermal potential is highly sensitive to NP size, size distribution, shape, composition and coating. For this reason, significant efforts have been made to optimize and standardize synthesis and functionalization protocols, allowing for improved heating capability, stability and biocompatibility of SPIONs, as well as of a wide range of different MNPs [44,66,67].

Intensive research has been conducted on preparing MNPs using different synthesis approaches, affording a plethora of different NP morphologies, including nanospheres, plates, tetrahedrons, cubes, concaves, octopods and multi-branched MNPs [68]. The most commonly used protocols consist of “bottom-up” synthetic methods entailing the build-up of MNPs from smaller constituents, generally following the nucleation and growth model [69]. Numerous synthesis routes have been established to prepare SPIONs (mainly magnetite and maghemite NPs), with chemical co-precipitation and thermal decomposition being among the most widely used [44,69]. Co-precipitation of iron salts is generally considered the most efficient method for SPION production, as it is inexpensive and produces NPs readily dispersible in water. It consists of the simultaneous precipitation of Fe^{2+} and Fe^{3+} in aqueous solutions, initiated by adding a base. This method uses cheap chemicals and can be performed at moderate temperatures (< 60 °C). Particle size and magnetic properties can be controlled by adjusting experimental parameters such as stoichiometry, temperature and pH [69]. Nonetheless, this method is known to generate NPs with relatively low magnetization and heterogeneous size distribution, as well as aggregate formation. This poses a significant limitation for their biomedical and thermal applications. Alternatively, thermal decomposition has been shown to yield monodisperse MNPs with tunable size. It uses NP precursors, such as ferric acetylacetonates, in high-boiling-point organic solvents (*e.g.* oleylamine, octadecene, *etc.*) [60,61]. For instance, Demortière et al. prepared iron oxide nanocrystals *via* thermal decomposition of $Fe(oleate)_3$ in a high-boiling point solvent, using oleic acid as a stabilizing agent. They demonstrated the influence of the type of solvent and the ligand/precursor ratio on NP size, yielding SPIONs ranging between 2 nm to 14 nm (Fig. 4) [70]. Similarly, Wetterskog et al. demonstrated that monodisperse iron oxide nanocubes and nanospheres with well-defined sizes (between 5 and 27 nm) can be synthesized *via*

Table 2|
Summary of recent examples of MNPs designed for NP-MTT hyperthermia *in vitro* and/or *in vivo*, with corresponding NP physicochemical *characteristics*, AMF parameters and SAR values. Adapted from [44].

Type of MNP	Core size (nm)	Coating	Field		SAR (W/g)	Temperature (°C)	Cancer type	Application	Tested		Reference
			Frequency (kHz)	Strength (kAm^{-1})					*In vitro*	*In vivo*	
Fe_3O_4 NP	22	FA	150	11.96	37.6	↑ 20–25	Murine breast cancer	MTT	×	×	[76]
Fe_3O_4 nanorings	70	mPEG	400	58.8	3050	44	Breast cancer	MTT	×	×	[77]
Fe_3O_4 nanocubes	19	PEG	520	29	2452	43	Epidermoid carcinoma	MTT	×		[78]
$Mn_{0.6}Zn_{0.4}Fe_2O_4$ nanospheres	8	Polymer	114	62.8	1018	42.3	Ovarian carcinoma and hepatocellular carcinoma	MTT + CT		×	[79]
Fe_3O_4 nanoellipsoids	92	OA-DHCA	360	43.7	1003	43.5	Breast cancer	MTT	×		[80]
$Mn_XZn_{1-X}Fe_2O_4$ nanospheres	8	mPEG-PCL	114	115.1	1002	43	Breast cancer	MTT	×		[81]
Zn ferrite nanospheres	15	Polymer	410	1.8	872	60	Breast cancer	MTT		×	[82]
$Fe_{0.6}Mn_{0.4}O$ nanospheres	100	mPEG	366	31.8	535	↑ 20	Breast cancer	MTT	×	×	[83]
Fe_3O_4 nanospheres	10	PPy-PEG-FA	230	8	487	44	Multiple myeloma	MTT + CT		×	[84]
$MnFe_2O_4$ nanospheres	31	–	765	23.9	400	↑ 5	Sarcoma	MTT	×		[85]
Mn ferrite nanoassembly	50	SiO_2	250	33.3	375	42–45	Cervical cancer	MTT	×		[86]
Mn-Zn ferrite nanospheres	8	PEG	390	12	324	43	Macrophages	MTT	×	×	[87]
Fe_3O_4 nanospheres	6	Alg	780	19	308.4	42.5	Hepatocellular carcinoma	MTT	×	×	[88]
Fe_3O_4 multicores	30	PEG	473	12	265	–	Glioblastoma	MTT	×		[89]
Fe_3O_4 multicores	22	Polymer	173	25	264.5	↑ 5–6	Epidermoid carcinoma	MTT		×	[90]
Fe_3O_4 nanospheres	8	Thiolated-PEG	230	8	248	↑ 6	Multiple myeloma	MTT		×	[91]
Fe_3O_4 nanospheres	9	SiO_2-polymer	105	18	178.5	–	Murine melanoma	MTT + CT		×	[92]
Fe_3O_4 nanospheres	10	PEG-PANI	265	26.7	120	43	Murine fibrosarcoma	MTT	×		[93]
Fe_3O_4 nanospheres	10–20	SiO_2	250–265	–	111	43	Cervical cancer	MTT	×		[94]
Fe_3O_4 nanospheres	20	BSA	512	10	109.8	↑ 5	Glioblastoma	MTT	×	×	[95]
Fe_3O_4 nanospheres	50–70	HA	307	50	85	45	Osteosarcoma	MTT	×		[96]

Abbreviations: FA – Folic Acid; PEG – Polyethylene glycol; CT – Chemotherapy; OA – Oleic Acid; DHCA - 3,4-dihydroxyhydrocinnamic acid; mPEG-PCL - poly(ethylene glycol)-b-poly-(ε-caprolactone); PPy – Polypyrrole; SiO_2 – silica; Alg – Alginate; PANI – Polyaniline; BSA – Bovine serum albumin; HA – Hydroxyapatite; ↑ - Temperature increase.

thermal decomposition. The authors reported that size and shape were highly dependent on the purity of the reactants, ratio of oleic acid/sodium oleate, temperature, and rate of temperature increase [71]. Lastly, shape control of IONPs *via* thermal decomposition was demonstrated by Zhou et al., who synthesized monodisperse IONPs with numerous shapes, including concave NPs, cubes, tetrahedra and plates [72].

Besides size, shape and composition, MNP surface features are crucial for overall MTT efficiency. Colloidal stability in aqueous solution and under physiological conditions is one of the critical steps in NP design, as it is essential for biological applications. However, most MNPs are synthesized in organic solvents (*e.g. via* thermal decomposition), and water-soluble MNPs generally present low colloidal stability. Hence, surface modifications using hydrophilic and biocompatible polymers are required [44]. Polymers are the most commonly used functional moieties to improve the stability and biocompatibility of NPs. Functionalization protocols using polyethylene glycol (PEG), polyvinyl alcohol (PVA), polyacrylic acid (PAA), dextran, and chitosan are well established and have been proven to reduce aggregation, increase blood circulation time, reduce toxicity and increase stability [67]. The type of ligand, its molecular weight, and the coating thickness need to be carefully considered, as they have been shown to impact the heating rates and SAR values of MNPs [67]. Liu et al. produced highly monodisperse PEG-coated SPIONs to investigate the effect of surface coating on the SAR. Their findings showed that a thin coat of a lower molecular weight polymer resulted in up to a 2.5-fold increase in SAR values [73].

Silica coating is another common strategy to improve NP performance. Moreover, SiO_2 can provide a useful and biocompatible binding layer for various biological molecules, including tumor-targeting ligands. Nonetheless, heat conduction through the silica shell might decrease heat outflow and heating efficiency in hyperthermia. Consequently, shell thickness is crucial for optimal heat generation [67,74]. The use of targeting moieties has been widely studied for actively targeted cancer therapies, promoting specific binding of the NPs to cancer cell biomarkers and consequent lower healthy-cell toxicity. Surface functionalization of MNPs boosts their potential in biomedical applications and is relatively simple to achieve, often by ligand exchange or ligand addition processes. Antibodies, peptides (*e.g.*, RGD), proteins (*e.g.* transferrin) and small molecules (*e.g.*, folate) are well-described examples of targeting ligands that can be conjugated to NPs to improve their specificity towards cancer cells [44,75]. Recently, Soleymani et al. used folate-conjugated IONPs as theranostic agents for simultaneous breast cancer therapy and MRI imaging in mice xenografts [76]. The functionalized MNPs showed good biocompatibility both *in vitro* and *in vivo*, and targeting ability was demonstrated in a mouse model. Results *in vivo* also revealed that tumor-bearing mice showed significant tumor regression upon AMF activation (f = 150 kHz and H = 9.9 kA/m) compared with mice subjected to NP administration or AMF alone, showing the MTT potential of the functionalized NPs (Fig. 5).

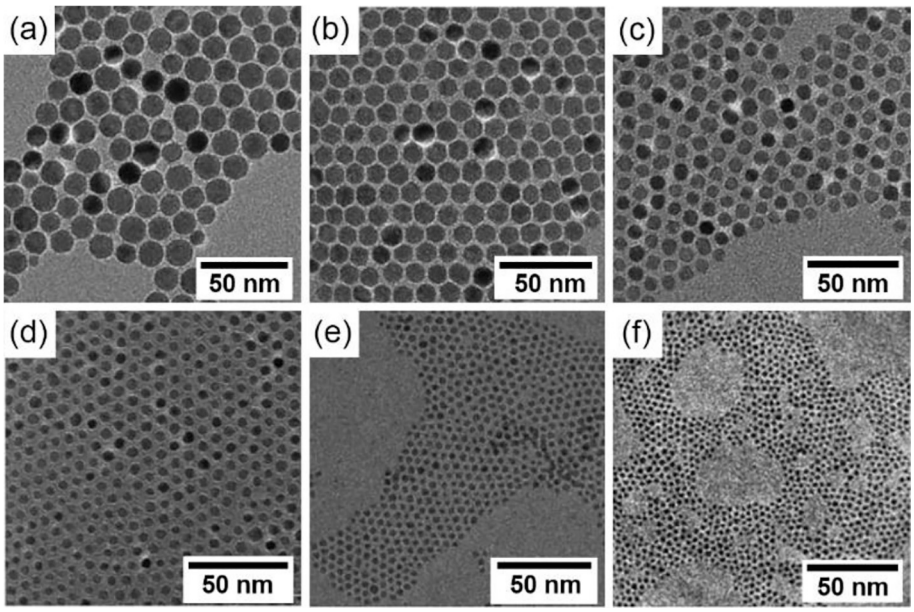

Fig. 4|. Transmission Electron Microscopy (TEM) images of iron oxide nanocrystals obtained using different high-boiling point solvents and ligand/precursor ratios (r). (a) 14 nm nanocrystal, prepared using eicosane and $r = 1$; (b) 11 nm nanocrystal, prepared using di-n-octylether and $r = 2$; (c) 9 nm nanocrystal, prepared using dibenzyl ether and r = 1; (d) 5 nm nanocrystal, prepared using di-n-octyl ether and $r = 0.3$; (e) 3.5 nm nanocrystal, prepared using hexadecene and $r = 0.5$; f) 2.5 nm nanocrystal, prepared using di-n-hexyl ether and $r = 0.5$. Reprinted from [70].

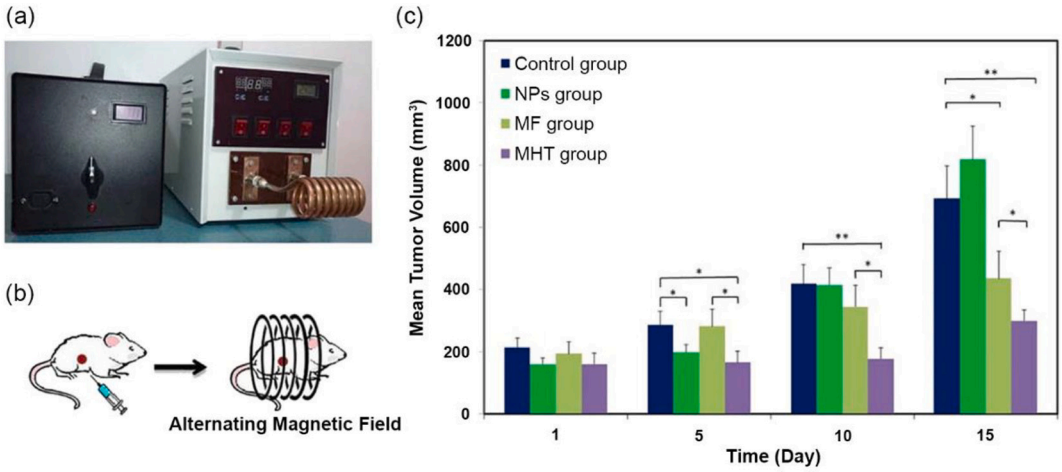

Fig. 5|. (a) NP-MTT unit used for *in vivo* experiments; (b) schematic representation of *in vivo* MTT on mice; (c) mean tumor volume *vs* days after treatment for the different groups. Control group consists of untreated mice, NPs group was intraperitoneally administered with FA@Fe_3O_4 NPs, without AMF activation, MF group was only exposed to AMF, and the MHT group was administered with NP injection and subjected to AMF treatment. (*) indicates $p < 0.05$, (**) indicates $p < 0.005$. Reprinted from [76].

2.2. NP-mediated Photothermal therapies

Photo-induced thermal therapies have received increased attention as noninvasive cancer therapies because of their potential for selective tissue heating using external laser irradiation [97]. Traditional molecular photothermal agents (PTAs) generate heat upon photoexcitation from the ground state (S_0) to the excited state (S_1, higher energy state), followed by the release of vibrational energy in the form of heat (non-radiative decay) [98]. However, molecular PTAs can have low photothermal conversion efficiency (PCE) and tumor accumulation, requiring high laser power and PTA concentration to achieve the desired therapeutic effects (PCE takes into account both light absorption efficiency and subsequent quantum yield of non-radiative relaxation). This raises side-effect concerns and limits clinical potential [20]. Owing to their comparatively high PCE and accumulation at the tumor site, the use of NPs reduces the total light energy required to achieve ablative temperatures. This decreases the chance of inadvertently heating the surrounding tissue and minimizes off-target toxicity [98,99].

For a given type of NP, therapeutic effectiveness can be optimized by tuning NP concentration, irradiation time, and laser intensity [100,101]. Additionally, the use of light sources working in the so-called biological windows (BWs) for PTT not only promotes deeper light penetration and allows for deep tissue treatments, but also limits off-target heating of healthy tissue. The different BWs, found within specific ranges in the near-infrared (NIR) region, allow for maximal light penetration due to minimal scattering and/or absorption by biological components (Fig. 6a). At these wavelengths, biological tissue becomes virtually transparent and light-tissue interactions are minimized [102]. While there is some disagreement in the literature on the definitions of BWs, in this review, we assume the existence of three different BWs (Fig. 6b).

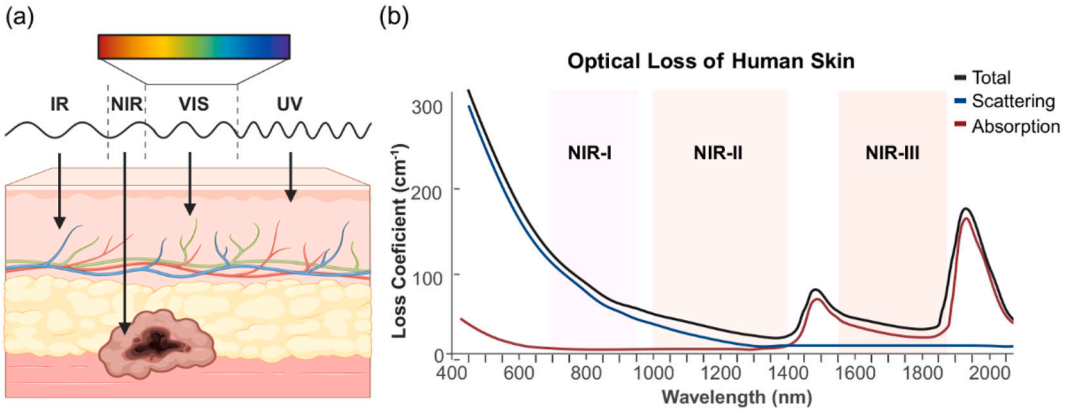

Fig. 6|. Schematic representation of the biological transparency windows exploited for biomedical applications. (a) Light in the visible range of the spectrum strongly interacts with biological tissue (strong absorption and scattering), hindering deep light penetration. In the NIR range, light-tissue interaction is significantly lower, and the tissue is virtually transparent to light, enabling deeper tissue penetration. Adapted from [106]. (b) These wavelengths are known as biological windows (NIR—I, 700–950 nm; NIR-II, 1000–1400 nm; NIR-III, 1550–1870 nm) and can be exploited to develop improved NP-PTT. Adapted from [104,107]. (Image created with BioRender.com).

The first window (NIR-I/I-BW), ranging between 700 and 950 nm, corresponds to the gap between the visible absorption bands of hemoglobin and melanin, and the water absorption band at 950 nm. Within the NIR-I region, light can reach tumors located 2–3 cm under the skin. While absorption is low, light scattering off cell-scale structures is still relatively high [103]. The second BW (NIR-II/II-BW) lies between 1000 and 1400 nm, and is bound by the sharp water absorption peak at ~1450 nm. The third BW (NIR-III) is found between 1550 and 1870 nm and is flanked by high absorption bands from water at 1450 nm and above 1800 nm [104,105]. In the NIR-II and NIR-III windows, light displays a maximum penetration ability of around 10 cm as both absorption and light scattering are low [18,103].

The advantages posed by NP-PTT have motivated the design of a wide range of nanomaterials suitable for PTT. These nanomaterials can be categorized into different groups with distinct morphology, heating mechanisms, efficiency, and spectral ranges. Factors such as shape, size, and composition of NPs affect their light absorption, and research has focused on optimizing these parameters to improve NP-PTT. PTT-suitable nanomaterials must be biocompatible, stable in physiological fluids and highly optically-absorbent. Furthermore, they should display tunable surface features to allow conjugation of different moieties for selective therapies [98,108–110]. Examples of efficient NPs for PTT include metallic NPs and their oxides (such as gold, silver and iron oxide NPs), carbon-based NPs [including carbon nanotubes (CNTs) and graphene NPs], silica NPs, semiconducting nanocrystals, rare earth ion-doped nanocrystals, polymeric NPs and hybrid NPs [102,111].

Various studies have been carried out on NP-PTT, and different nanomaterials have been tested *in vitro* and *in vivo*. These studies focus on improving NP-PTT by finely tuning NP physicochemical properties (*i.e.*, shape, size, surface composition), concentration, PCE and targeting ability. Understanding these properties is paramount for the optimization of light exposure parameters, including wavelength (λ), exposure time (*t*) and power density (W/cm^2) [99]. Some examples of recent and relevant studies are compiled in Table 3. In this next section, we will describe the most commonly used nanomaterials in PTT, including gold-, iron-, carbon-based- and polymeric NPs. Other nanomaterials for PTT applications have been extensively reviewed elsewhere [98,109,110,112].

2.2.1. Gold Nanoparticles

Gold NPs (AuNPs) were first introduced in the 1850s when Michael Faraday showed that gold salts could be reduced in the presence of organic ligands to form stable colloidal dispersions of gold particles. 170 years later, almost perfect control over size, shape, and homogeneity of AuNP samples has been attained. The unique properties of AuNPs make them appealing candidates for a wide range of biomedical applications, including sensing, cellular imaging, and cancer therapy. First, being an inert, noble metal, Au does not react with biological tissues, resulting in high biocompatibility. This has led to FDA approval for numerous Au-based nanoformulations in biomedical applications, with many others undergoing clinical trials [113]. Furthermore, AuNPs present easily scaled-up synthesis, high structural control, tunable light absorption capability in the BWs, and can be easily functionalized with thiol-based ligands, making them ideal candidates for targeted cancer PTT [114].

In PTT, AuNPs can induce heat upon laser irradiation due to their localized surface plasmon resonance (LSPR) [97]. The LSPR phenomenon consists of collective waves of the free electrons excited by characteristic light wavelengths, which eventually decay into heat [99,102]. When the incident light interacts with the conduction electrons at the metal-dielectric interface, it leads to coherent surface plasmon oscillations (resonance effect). Upon surface plasmon excitation, nonradiative decay of the electron gas transforms photon energy into thermal energy, leading to local heat generation [97,115].

AuNPs can be synthesized in a wide range of well-characterized shapes, including solid gold nanospheres, nanorods (AuNRs), nanostars (AuNSs), nanoshells and nanocages [109]. By adjusting the shape and size of these NPs, LSPR wavelengths can be tuned to the NIR to increase tissue penetration and minimize off-target damage by adjusting the NP size, shape or composition [13,115]. The distinct length and width of gold nanorods (AuNRs) make them particularly interesting. It has been shown that the long wavelength LSPR peak position in AuNRs varies almost linearly with the aspect ratio. Hence, by changing this ratio, it is possible to tune the maximum wavelength LSPR peak to the NIR region while ensuring an optimal size for cellular uptake (< 200 nm, Fig. 7) [116,117]. This presents a crucial advantage for AuNRs compared to spherical AuNPs, which display an LSPR peak in the visible range of the spectrum (400–600 nm), hindering light penetration and clinical use [112,118]. In addition, AuNRs have shown superior heat conversion upon NIR light excitation to most AuNPs and a high blood circulation half-life, increasing the chances of specific passive tumor accumulation [13]. AuNSs have also been pointed out as interesting candidates for NP-PTT, due to their tunable LSPR in the NIR and high PCE [119]. However, compared to NRs, the spike features reduce their colloidal stability and make their synthesis and application more challenging. These spikes are also sensitive to oxidation, leading to a lower stability of AuNSs [120,121].

While significant efforts are being made to enhance light-to-heat

Table 3|
Summary of recent examples of NPs designed for NP-mediated cancer PTT *in vitro* and/or *in vivo*, with corresponding NP physicochemical characteristics, laser source parameters and PCE values (when available).

Type of MNP		Size (nm)	Coating	Laser irradiation			PCE (%)	Temperature (°C)	Cancer type	Application	Tested		Reference
		d or L × d		Wavelength (nm)	Power (W/cm^2)	Exposure time (min)					*In vitro*	*In vivo*	
Inorganic NPs	AuNRs	97 × 17, 87 × 15, 70 × 11.5, 60 × 10.5	PEG-LF	980	0.5	1	–	65.7	Hepatocellular carcinoma	PTT	×	×	[123]
	AuNRs	28 × 9	Nes-PEG	800	0.5	7 or 4	–	67	Glioblastoma	PTT	×		[136]
	HAPP (AuNS@HMS)	~200	PEG	808	1.2	10	–	70.2	Glioma	PTT	×	×	[137]
	AuNSs	80	ICG-BSA	808	1	5	–	63.9	Glioblastoma	PTT	×		[138]
	AuNR@SiO_2	59 × 9.3	ICG	808	0.8	6	–	63.6	Lung Cancer	PTT and PDT	×	×	[139]
	AuNRs/nHA	48 × 12	PEG	808	0.99	5	–	57.6	Osteosarcoma	PTT	×	×	[140]
	AuNRs	55.1 × 14.1	HA	808	2	10	–	84	Breast Cancer	PTT and PDT	×	×	[141]
	BSA-Au Nanoshell	151	BSA-Gd	808	1.5	5	21.8	~ 60	Breast Cancer	PTT and PDT	×	×	[142]
	AuNR	> 20	SH-CL90	808	2	10	22.2	48.5	Liver, Breast and Lung Cancer	PTT	×	×	[143]
	Au nanospheres@Pt	42.4	HA	808	1.5	10	63.5	↑ 30	Murine Melanoma	PTT	×	×	[144]
	TMZ@AuNPs	45.9	Anti-EphA3	NIR	2	5	–	47	Glioblastoma	PTT and CT	×	×	[145]
	Fe_3O_4@DEX	160	PGEA	1064	1	5	–	↑ 19	Breast Cancer	PTT	×	×	[146]
	rGO-Fe_3O_4	4–20	–	804	1	5	–	43.1	Cervical Cancer	PTT	×		[147]
	FITC- Clustered IONPs	103–107	MPEG	808	1	5	71	78.5	Lung Cancer	PTT	×	×	[148]
	Carbon nanodots	4.7	–	650	0.41	10	42	51.9	Liver Cancer	PTT	×		[149]
Organic NPs	SWCNT	0.8 nm × 1500 μm	ANXA5	980	1	175 s	–	54	Breast Cancer	PTT and immunostimulation		×	[150]
	ICG-BSA NCs	35	–	808	1	10	–	↑ 25	Breast Cancer	PTT	×	×	[134]
	PANi@PVP	30–50	PVP	808	2	15	–	45–49	Hepatocellular carcinoma	PTT	×	×	[133]
	IR820-PLGA NPs	60	–	808	1.5	5	–	>42	Breast Cancer	PTT	×	×	[151]

Abbreviations:- PCE – photothermal conversion efficiency; AuNR – Gold Nanorod; PEG – polyethylene glycol; LF – Lactoferrin; AuNS - Gold Nanostar; Nes – Nesprin; HAPP - AuNS-coated, perfluorohexane (PFH)-encapsulated hollow mesoporous silica nanocapsule; ICG - Indocyanine green; PDT – Photodynamic therapies BSA – Bovine Serum Albumin; SiO_2 – Silica; nHA – Nanohydroxyapatite; SH-CL90 – thiolated lemon polysaccharide; Pt – Platinum; TMZ - Tomozolamide; CT – Chemotherapy; PGEA – Polycation; rGO – reduced graphene oxide; Fe_3O_4 – magnetite; FITC – NIR-797 isothiocyanate dye; MPEG – PEG-block-copolymer; SWCNT – Single-walled carbon nanotubes; ANXA5 – annexin A5; PANi - Polyaniline; PVP - Poly(vinylpyrrolidone); IR820 - NIR-absorbing dye; PLGA - poly(lactic-*co*-glycolic acid).

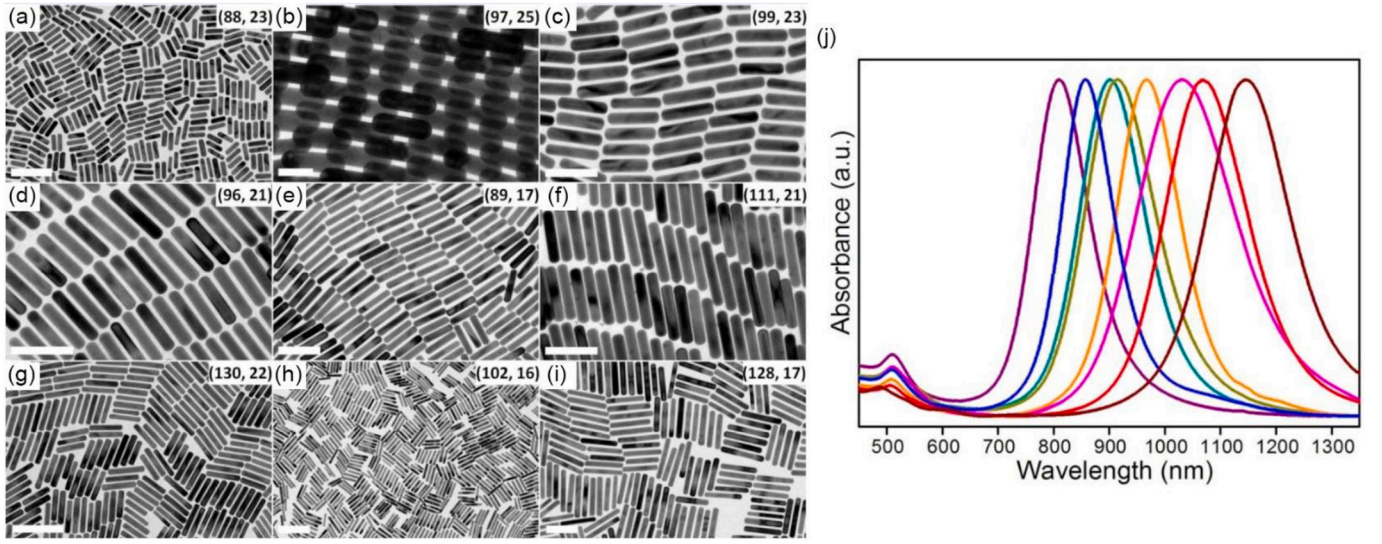

Fig. 7|. TEM images of AuNRs with different aspect ratios (a-i). Inserts are the average length and diameter in nm. Scale bars: (a) 200 nm, (b) 50 nm, (c-f) 100 nm, (g-h) 200 nm, (i) 100 nm; (j) Normalized extinction spectra of AuNRs a, c-i. As the aspect ratio increases, the LSPR extinction peak shifts towards longer wavelengths. Reprinted from [117].

generation by AuNPs, enormous focus has been given to improving NP performance in cancer cells. NP physicochemical properties and functionalization strategies have been exploited for higher biocompatibility, colloidal stability and targeting and accumulation at the tumor site [122]. Yang et al. studied the impact of size and surface ligand of AuNRs on tumor accumulation and PTT efficacy on liver cancer. AuNRs with similar aspect ratios and LSPR peaks, but tunable width and lengths, were used to evaluate the influence of NP dimension on cellular uptake and PTT. The AuNR surface was then modified with different moieties. Results showed that AuNRs with a medium size (70 × 11.5 nm), modified with targeting moieties (lactoferrin), exhibited the fastest cell internalization and PTT efficacy in cells. Tumor accumulation and thermal ablation were validated on mice xenograft, suggesting the synergistic effect of NP size and surface coating on anti-tumor performance [123]. Yang et al. performed a systematic study on the effect of AuNP shape in cancer PTT. They compared the performance of Au nanospheres, nanorods and nanostars with similar surface functionalization (mPEG-SH). Results showed that all NPs generate heat upon 808 nm laser excitation, and nanostars showed the highest PCE (Fig. 8). Observations in cells corroborated these conclusions: upon laser irradiation (10 min, 300 mW/cm^2), Au nanostars induced the highest (a) temperature rise, (b) PCE, and (d, e) cell mortality. Therefore, this study suggests that the developed Au nanostars hold the most promise out of the tested AuNPs [115].

2.2.2. *Iron Oxide Nanoparticles*

Besides their application as heat-mediators in MTT, metallic NPs such as IONPs, have also been reported to generate heat upon NIR light irradiation. IONPs present a unique advantage as PTT-mediators since their magnetic nature can address NP accumulation at the tumor site *via* external magnetic field application [109,124]. However, IONPs display low PCE, requiring power densities above the safety limit to achieve tumor ablation [125,126]. Some strategies have been explored to improve IONPs PCE. For instance, hybrid nanocomposites have been designed where materials with high PTT efficiency are conjugated with the surface of IONPs. Lin et al. used NPs coated with isocyanine green (ICG), a well-described photosensitizer, to achieve photothermal-mediated chemotherapy of U87MG tumor cells [127,128]. Neshastehriz et al. demonstrated that Au@IONPs composites act as powerful thermal-radiosensitizers, capable of inducing apoptosis in gliomas [129].

2.2.3. *Carbon-based Nanostructures*

Carbon-based nanostructures (CNSs), such as single-walled carbon nanotubes (SWCNTs), multi-walled carbon nanotubes (MWCNTs) and graphene structures, have also been explored as photo-absorbers for PTTs, owing to their high surface area, high chemical stability, and broadband light absorption. CNSs can generate heat due to the excitation of π electrons and subsequent relaxation to their ground states, *via* nonradiative relaxation processes caused by defective carbon-ring structures [108]. Graphene oxide (GO) nanosheets have been reported to have excellent PCE. Liu et al. developed PEGylated GO nanosheets (NGS-PEG) with strong optical absorbance in the NIR region for *in vivo* PTT against breast cancer. Ablative temperatures around 50 °C were achieved upon 808 nm laser irradiation, resulting in cell death [130]. Despite their potential, carbon-based NPs have been reported to show concentration and size-dependent toxicity, which can limit their clinical potential.

2.2.4. *Polymeric Nanoparticles*

Another class of NPs that can be used as carriers for PTAs in NP-PTT are polymeric NPs. Heat-generating molecules can be loaded inside the polymeric structures *via* electrostatic interactions or covalent bonds, and delivered to the tumor site, where temperature increase is then promoted *via* laser activation [109,131]. Polymeric NPs can be synthesized using natural polymers (such as hyaluronic acid, albumin, polydopamine, and chitosan), or synthetic polymers [including Poly-L-lactic acid, polyethylene glycol, poly(lactic-*co*-glycolic acid), polyaniline and polypyrrole], and have been widely studied due to their high biocompatibility and biodegradability [109]. Conjugated polymers, such as polyaniline and polypyrrole, have also been reported to generate heat *via* excitation of π electrons, as previously described for the carbon-based nanostructures [132]. Wang et al. showed that polyaniline NPs shelled with poly(vinylpyrrolidone) had excellent photothermal efficiency, and observed anti-tumor potential both *in vitro* and *in vivo* [133]. Recently, An et al. designed a phototheranostic nanoformulation consisting of bovine serum albumin (BSA) NPs loaded with ICG for guided NIR imaging and PTT. Results showed that the BSA-ICG complex has higher photoluminescence quantum yield (PLQY) and *in vivo* tumor accumulation efficiency than free ICG, contributing to improved NIR imaging. Data also showed improved PTT efficiency, and high biocompatibility for improved NP-PTT [134].

In summary, even though significant progress has been made in NP-

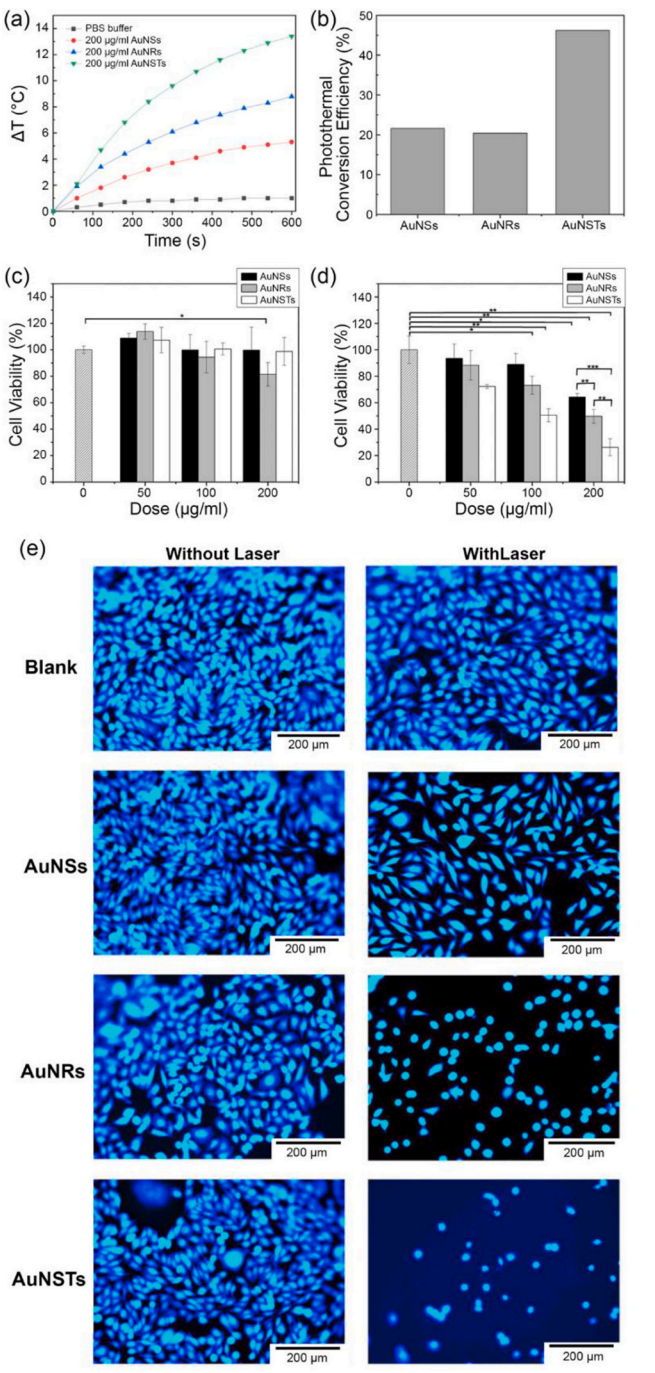

Fig. 8|. (a) Temperature increase triggered by the different AuNPs under 808 nm irradiation (300 mW/cm^2); (b) Photothermal conversion efficiency of the AuNPs in PBS buffer at a concentration of 200 μg/mL, demonstrating a higher photothermal potential of Au nanostars over nanorods or nanospheres; (c) Viability studies of PC-3 cells after incubation with different PEGylated AuNPs, showing low cytotoxicity for the studied concentrations; (d) Cell viability after NP incubation and laser irradiation (300 mW/cm^2); (e) Fluorescence images of PC-3 cells treated with PBS (control) or 200 μg/mL AuNPs without (left) and with (right) laser irradiation. Viable cells are shown in cyan upon staining with CytoCalcein Violet 450 (Ex/Em = 405/450 nm). AuNSs, AuNRs and AuNSTs stand for Au nanospheres, nanorods and nanostars, respectively. Data were shown as mean of three identical tests ($n = 3$) ± standard error, (*) $p < 0.05$, (**) $p < 0.01$, (***) $p < 0.001$. Reprinted from [115]. (For interpretation of the references to colour in this figure legend, the reader is referred to the web version of this article.)

HT, numerous challenges must be overcome to improve clinical prospects. Research has been focusing on tackling colloidal stability, heating capability, targeted therapeutic action, and off-target toxicity. However, a better understanding of the underlying interactions between NPs and cells is required, as well as a thorough study of the pharmacokinetics and biodistribution of the NPs [12]. The long-term toxicity of NPs also needs to be further investigated in preclinical platforms to improve the potential for clinical translation [135].

2.3. Combination therapies using NP-mediated hyperthermia

As previously outlined, NP-HT as a standalone approach has exhibited strong therapeutic potential. However, NP-PTT is also emerging as a powerful adjuvant to traditional cancer therapies, promoting higher treatment success rates by combining the strengths of multiple approaches [152]. Elevated temperatures have a synergistic effect with chemotherapy, acting as a chemosensitizer. Improved blood flow and tumor oxygenation resulting from HT can enhance drug accumulation and cellular uptake, while also inhibiting DNA repair pathways and accelerating drug toxicity [16]. Encapsulating drugs inside NPs can improve their solubility, thereby improving their antitumor action [108]. In addition, NPs with simultaneous hyperthermal and drug delivery ability can be used for heat-triggered drug release at the tumor site, improving both selectivity and efficacy [153]. Increased vascularization results in better oxygenation of the hypoxic core of the tumor – which is generally resistant to radiation. The higher amount of oxygen leads to the enhanced generation of the free radicals responsible for cell death. Thus HT can be used as a radiosensitizer for enhanced radiotherapy [108,154]. HT can also act as an adjuvant to immunotherapies, due to thermally induced metabolic changes that trigger immune response [17].

Magnetic NPs have been reported by several studies to be promising platforms for combined therapies. Lee et al. developed a magnetothermal responsive formulation comprising doxorubicin (DOX) encapsulated supramolecular MNPs to achieve an on-demand drug delivery upon AMF application. Results *in vivo* showed significant tumor shrinkage over the course of 15 days when AMF was applied (500 kHz, 37.5 kA·m^{-1}, 10 min) [155]. Ren et al. used MNPs as adjuvants to radiotherapy. Mn—Zn ferrite NPs (MZF) were modified using hyaluronic acid (HA) as a tumor-targeting agent, owing to receptor-ligand specificity of HA and the CD44 cell receptor overexpressed by tumor cells. Under AMF, HA–MZF NPs led to a local temperature increase, which led to improved tumor oxygenation and higher radiotherapeutic potential. *In vitro* and *in vivo* studies revealed high biocompatibility and tumor-targeting ability. The authors showed that the combined therapeutic approach can induce higher cell death than HT or radiotherapy alone [156]. In a recent study, Mei et al. used IONPs (Fe_3O_4) as a delivery system to carry indocyanine green (ICG) and an immunostimulator, R837 hydrochloride. The resulting NPs could be simultaneously used for MIR imaging and anti-tumor therapy. Under NIR irradiation, tumor ablation was triggered, which led to tumor-associated antigen release, inducing the body's response to tumor cells. R837 release also significantly improved immune activation. Together, PTT and immunotherapy improved tumor destruction, inhibiting metastasis and recurrence [157].

Metallic NPs as PTT agents are also garnering attention for their potential in combined therapies. For instance, Mehtala et al. studied the synergistic effects of chemotherapeutic cisplatin and AuNR-mediated hyperthermia. *In vitro* results revealed an 80% increase in drug efficacy against ovarian carcinoma and *in vivo* studies showed significant tumor growth suppression upon combined therapeutic action [158]. AuNPs have also been used in combination with radiotherapy. Shen et al. designed PEGylated hollow gold NPs (mPEG@HGNPs) for combined PTT and radiotherapy against breast cancer. Data showed significant thermo-radiosensitive efficiency and synergistic anti-tumor effects. mPEG@HGNPs also proved extremely useful for CT imaging *in vivo*

[159]. Wu et al. designed a photothermally controlled drug release system for synergistic photo-chemical breast cancer therapy (Fig. 9). Anti-tumor efficacy was compared in a breast cancer cell line (MCF-7) and multidrug resistant (MDR) human breast cancer cell line (MCF-7/ADR). AuNPs were shelled with mesoporous silica (AuNPs@$mSiO_2$) and DOX was loaded into the silica pores for chemotherapeutic action. The NPs were then functionalized with folic acid for targeted tumor uptake (AuNP@$mSiO_2$-DOX-FA, Fig. 9a, b). Their results showed a time-dependent DOX accumulation in the nuclei of both cell lines upon incubation with AuNP@$mSiO_2$-DOX-FA (Figs. 9c, d). Free DOX was only found to accumulate in MCF-7 cells, due to the MDR of MCF-7/ADR cells, showing the role of functionalized delivery systems in improving drug accumulation in the cancer tissue. The resulting formulation displayed high PTT efficacy, with a temperature increase of up to 51 °C after 6 min of 808 nm laser irradiation at 2 W/cm^2. More importantly, the thermal effect triggered drug release, leading to a significant decrease of viability to 9.7% and 16.9% in MCF-7 and MCF-7/ADR cells, respectively (Fig. 9e, f). This study showcases the synergistic potential of chemotherapy and PTT, particularly in overcoming multidrug resistant breast cancer [153].

Due to their NIR-to-heat conversion capabilities and straightforward surface chemistry for the conjugation of chemotherapeutic agents, carbon-based NPs offer another promising avenue [152]. Tu et al. designed silica-coated CNS/doxorubicin nanocomposites for breast cancer treatment. *In vitro* and *in vivo* studies showed heat generation and enhanced drug release upon NIR irradiation, with improved therapeutic ability when compared to PTT and chemotherapy alone [160]. Lipid-based NPs like liposomes are frequently employed as drug carriers due to their biocompatibility and high drug payload. Temperature-responsive liposomes can enable targeted drug release at the tumor site when combined with heat mediators which can consist of thermal NPs or other thermal agents, such as ICG [158]. Similarly, polymeric NPs, such as those made from poly(lactic-*co*-glycolic acid) (PLGA) and chitosan, provide biocompatible delivery systems for thermal mediators and/or other therapeutic agents [152].

Another approach towards combinatory therapy is using PTT to improve photodynamic therapies (PDT) [108]. PDT uses laser light excitation to trigger the formation of reactive oxygen species (ROS) by a photosensitizer (PS) [161]. At the tumor site, the PS, which may be a molecular dye or a nanocrystal, is excited using an external laser source. This leads to photon absorption and consequent excitation from the singlet ground state (S_0) to the singlet excited state (S_1). From the S_1, the photosensitizer can undergo intersystem crossing and convert into an excited triplet state (T_1). Electron transfer to oxygen from S_1, or energy transfer to oxygen *via* T_1, then leads to the formation of cytotoxic oxygen species, triggering cell death. Alternatively, the activated PS directly interacts with a biomolecule to produce ROS [108,162,163]. Heat generation by adjuvant NP-PTT can boost the effectiveness of PDT, increasing oxygen levels in tumors for higher ROS generation. Additionally, the encapsulation of PSs inside NPs can significantly improve their delivery into cells. In return, ROS can reduce the protective effects of certain proteins (heat-shock proteins) in cancer cells during PTT. Moreover, both PTAs and PSs can be activated using a single laser excitation, for simpler treatment courses [99]. An example of the synergetic effects of PTT and PDT is the study by Mei et al. where a photosensitizer (chlorin e6) was incorporated in hollow mesoporous MnO_2 NPs functionalized with folic acid (FA) for tumor-targeting capability. The resulting multifunctional NPs displayed pH-triggered Ce6 release at the tumor active site. Upon 660 nm laser irradiation, Ce6 promoted ROS generation, while 808 nm laser irradiation led to heat generation at the tumor site, further promoting Ce6 release and PDT therapeutic efficacy. *In vitro* and *in vivo* results demonstrated a higher anti-tumor efficacy for the combined ROS production and thermal-cumulative effect of the PTT-PDT therapy [164].

NP-HT has demonstrated impressive potential as an adjuvant strategy to numerous therapeutic approaches, making it a promising avenue for enhancing the efficacy of these therapies, while circumventing their side-effects. Despite promising preclinical results, further progress is needed for the clinical success of combination therapies. A better understanding of the relationship between HT and other approaches is required. In addition, it is paramount to unravel the effect of thermal dose as an adjuvant strategy to improve tumor response to chemo and radiotherapeutics, and PDT agents, as well as its effect on immune response. To do so, improved temperature monitoring techniques should be developed and applied [17].

2.4. Clinical translatability of NP-HT

While the prevalence of NPs in cancer hyperthermia has increased, relatively low bench-to-bedside translation is observed, and clinical implementation remains limited. Most NPs in clinical trials fail due to the low translatability of results obtained in preclinical studies (2D *in vitro* models and animal models) [165,166]. *In vivo,* NPs interact with several types of macromolecules in the bloodstream, and within the TME. These macromolecules can be adsorbed at the NP surface, forming a protein corona, which affects the physicochemical properties and stability of the NPs, leading to unpredictable therapeutic performance in the clinic. Limited accumulation at the tumor site and diffusion through the tumor stroma have also been pointed out as limitations of NP application in the human body [166]. Regarding NP-PTT, its implementation in clinical settings is also hindered by limited light penetration depth, and non-specific damage to healthy tissues near the target tumor site [167]. As previously described, most nanomaterials designed for NP-HT consist of metal or metal-oxide NPs. In spite of their potential, their clinical approval rate is often hindered by long-term biosafety concerns and accumulation in healthy organs, including the liver and spleen. A lack of standardized approaches to assess NP toxicity, biodistribution and clearance mechanisms poses a significant challenge in designing NPs that fulfill the regulatory requirements for FDA approval [167]. Furthermore, the large-scale production of these NPs is often costly, and suitable storage conditions can be hard to achieve [166].

Over the past two decades, only three different NP-HT systems have reached the clinical trial phase, including Magnablate® and Nanotherm® for magnetic HT, and AuroShell® for laser-induced HT. Magnablate® consists of an IONP suspension developed for NP-MTT of prostate cancer. These NPs (NCT02033447) underwent Phase 0 clinical trials with 12 participants, but no results are yet available. Nanotherm® is an aqueous suspension of amino silane-coated SPIONs, and has been clinically approved by the EMA for the thermal ablation of glioblastoma multiforme [168]. Nanotherm® has also undergone clinical trials for prostate cancer treatment, but the study was terminated due to insufficient enrollment (NCT05010759). Recently, a new trial has opened and is currently recruiting for the treatment of glioblastoma (NCT06271421). Regarding NP-PTT, no formulation has been clinically approved so far, and only one formulation has reached the clinical trials phase. AuroShell® is a gold-based formulation from AuroLase®. It consists of a PEGylated silica-gold nanoshell suspension (~ 150 nm diameter) designed for the laser-activated thermal ablation of head and neck solid tumors, metastatic lung cancer, and prostate cancers, upon intravenous administration [168]. For neck and head cancer treatment, intravenous NP injection was followed by one or more doses of NIR laser irradiation (808 nm) (NCT00848042). Participants were divided into three groups and subjected to different therapeutic parameters, namely NP concentration and laser power. Results indicate that 3 out of the 11 patients displayed severe adverse side-effects and all the remaining experienced mild side-effects. For the treatment of metastatic lung cancer, a single dose of AuroShell® was administered to promote thermal ablation of cancer cells (NCT01679470). However, to this date, no results have been made available. Lastly, Auroshell® is currently being tested in combination with an MRI/Ultrasound fusion technology for prostate cancer (NCT02680535). This study has been completed and then extended (NCT04240639), and is currently recruiting participants,

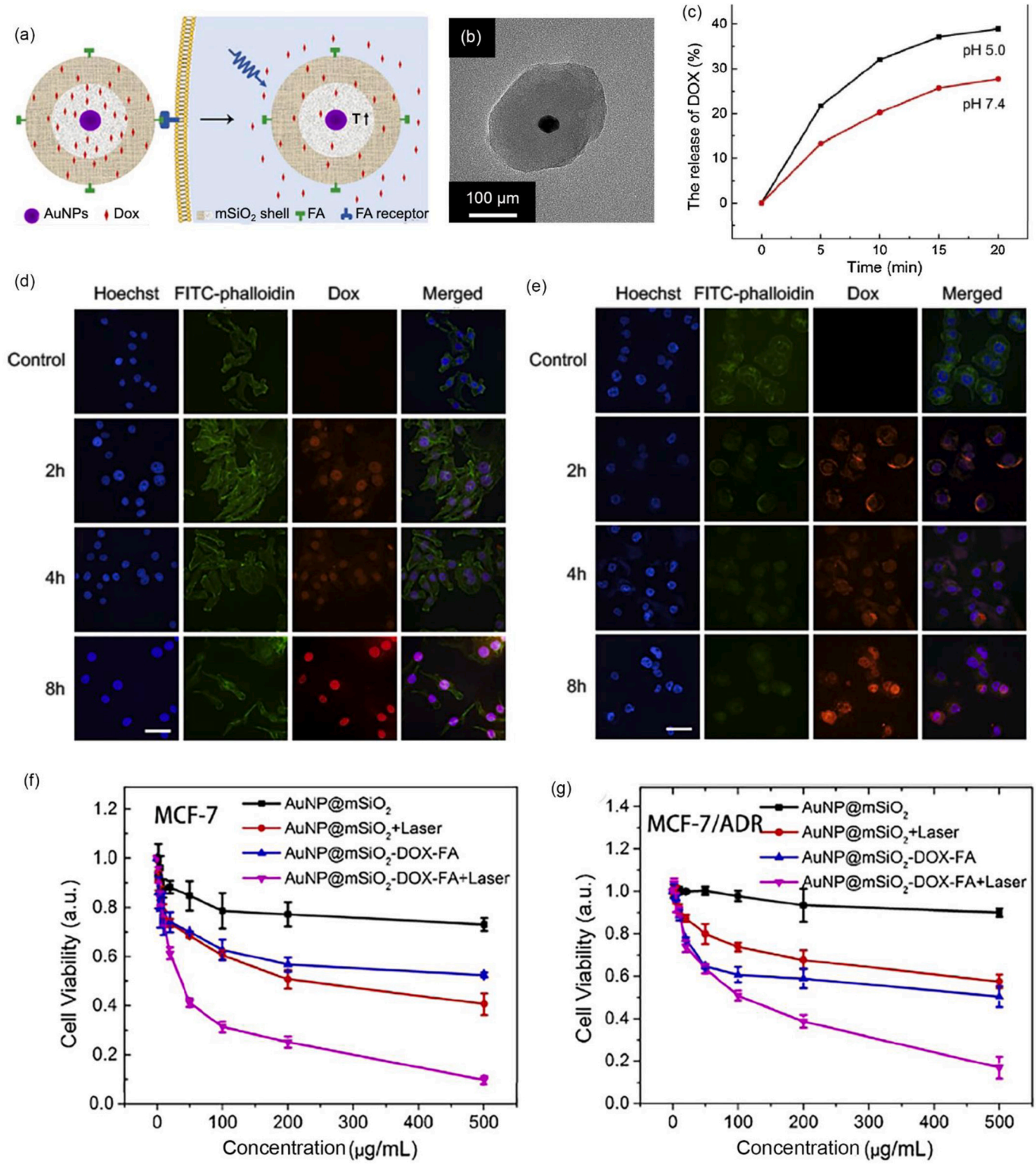

Fig. 9|. (a) Schematic illustration of the DOX-loaded Au-based nanoformulation (AuNP@mSiO$_2$-DOX-FA) for synergistic chemo-photothermal therapy; (b) TEM image of AuNP@mSiO$_2$-DOX-FA; Total internal reflection fluorescence microscopy images of (c) MCF-7 and (d) MCF-7/ADR cells incubated with AuNP@mSiO$_2$-DOX-FA (1 mg/mL) for 2, 4 and 8 h. Cells without AuNP@mSiO$_2$-DOX-FA were used as a control. The cells were treated with Hoechst 33258 and FITC phalloidin at room temperature to stain the nuclei and cytoskeletons. Scale bar: 50 μm; Viability of (e) MCF-7 cells and (f) MCF-7/ADR cells incubated with AuNP@mSiO$_2$ and AuNP@mSiO$_2$-DOX-FA nanoparticles for 24 h without or with laser irradiation (808 nm, 2 W/cm^2, 15 min). Error bars represent SDs of six separate measurements (n = 6). Reprinted from [153].

but no data could be found on the thermal tumor ablation. The currently ongoing clinical trials listed on clinicaltrials.gov database are summarized in Table 4.

Despite intense development, NP-HT still faces numerous challenges associated with suboptimal and heterogeneous NP distribution at the tumor site, low control over the temperature increase, and inaccurate temperature readout. This highlights the importance of implementing more robust and standardized preclinical techniques for NP evaluation, allowing for the fine-tuning of NP properties and, consequently, enhanced bench-to-bedside translation [31].

3. Temperature sensing

While systemically administered NPs provide a promising alternative to conventional HT approaches, several challenges remain in using nanoformulations in the clinic. One of the main hurdles is heterogeneous heat distribution within the tumor, as well as off-target temperature increase and consequent damage to surrounding healthy tissue. As shown in Fig. 1, precise temperature control is crucial to determine the effects on tumor inhibition. Irreversible cell damage and thermal ablation are achieved at temperatures exceeding 45 °C [4,9,13]. Between 40 and 45 °C, mild to moderate hyperthermia leads to reversible changes and enhanced cell sensitivity to other treatments such as chemo- and radiotherapy [15,16]. In view of the strong dose-effect observed for HT, an accurate temperature control within the tumor mass is essential for improved anti-tumor action. Simultaneously, temperature in the surrounding healthy tissue, should be kept within biologically safe levels (< 40 °C). To achieve this, methods to precisely monitor temperature changes within the tumor, with high spatial and thermal resolution, need to be applied during NP design, ensuring a higher clinical translation and safer therapeutic action [13].

3.1. Thermometry and dosimetry

Precise spatiotemporal temperature observation (*i.e.* thermometry) and accurate temperature profiling within the target area are key for the development of HT-based therapies. It allows for the adequate estimation of dose-effect relationship and maximizing therapeutic efficiency, while keeping side-effects at a minimum [5]. To date, most temperature sensors are based on contact thermometers, including thermocouples and fiber optic sensors [169]. These have been used as the gold standard temperature sensing methods in HT due to their accuracy (0.1 °C), straightforward use and low cost. Nonetheless, temperature readouts are achieved by direct contact with the tissue, requiring heat conduction and thermal equilibrium between the target site and the sensor. Contact thermometers are, therefore, highly invasive and limited to one specific point in the tumor [170–172]. Non-contact thermometry can surpass some of the limitations imposed by contact thermometry and includes a wide range of techniques. Some of the most used include infrared (IR) tomography, magnetic resonance thermometry (MRT), photoacoustic (PA), ultrasound tomography, computer tomography (CT), Raman scattering, interferometry and luminescence nanothermometry [172]. IR tomography, also known as thermal imaging, is the most widely used non-contact technique. It works by detecting emitted thermal radiation and converting it to a thermogram, a visual temperature distribution with both high thermal resolution (< 0.1 °C) and spatial resolution (~ 0.1 mm). However, it is limited by the emissivity of the tissue, and can only be applied to superficial temperature sensing, limiting its use in intratumoral thermal studies [169,173]. Recently, non-contact luminescent nanothermometers have been explored as an alternative to the traditional methods by providing real-time feedback of the local temperature with high thermal (0.1 °C), spatial (<10 μm) and temporal (<10 μs) resolution [172].

3.2. Luminescence Nanothermometry

Luminescent nanothermometers with high brightness in the NIR region have enabled performing thermal readouts even from deep within a tumor mass. Nanothermometry is based on the use of temperature-sensitive nanoscale materials that undergo measurable

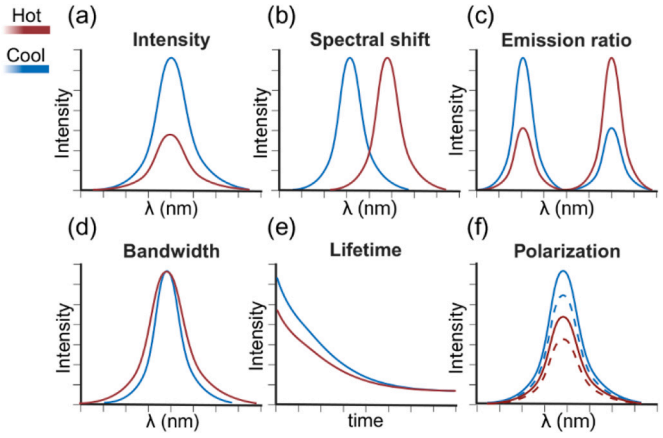

Fig. 10|. Fluorescence nanothermometry temperature sensing methods: (a) intensity, (b) spectral shift, (c) emission ratio (FIR), (d) bandwidth, (e) lifetime and (f) polarization-based luminescent thermometry. Adapted from [172,177]. (Image created with BioRender.com).

Table 4|
Summary of nanoparticle-mediated hyperthermia in clinical trials for cancer therapy as of May 2025. Data was collected from the clinicaltrials.gov database (data from 27/05/2024). Adapted from [168].

	ClinicalTrials.gov ID	NP Type	Cancer type	Status	Administration
NP-MTT	**NCT02033447** (2014-2015)	Magnablate®	Prostate Cancer	Early Phase I: Completed	Local Injection
	–	Nanotherm®	Glioblastoma Multiforme	Approved by EMA	Local Injection
	NCT05010759 (2021–2023)	Nanotherm®	Prostate Carcinoma	Terminated (inadequate enrolment)	Local Injection
	NCT06271421 (2024-present)	Nanotherm®	Glioblastoma Multiforme	Recruiting	Local Injection
NP-PTT	**NCT00848042** (2009–2016)	AuroShell®	Head and Neck Cancer	Completed	Intravenous
	NCT01679470 (2012-2016)	AuroShell®	Metastatic Lung Cancer	Terminated	Intravenous
	NCT02680535 (2016-present)	AuroShell®	Prostate Cancer	Completed	Intravenous
	NCT04240639 (2020-present)	AuroShell®	Prostate Cancer	Active, not recruiting	Intravenous

Abbreviations: EMA – European Medicines Agency.

modifications to their luminescence spectra in response to variations in temperature [174]. As depicted in Fig. 10, thermal readouts can be achieved through simple spectroscopic analysis, by deriving the temperature from changes in the emission spectra, including absolute intensity, spectral shifts, ratiometric changes, bandwidth, fluorescence lifetime or polarization (Fig. 10a-f) [175,176]. These readouts can be a consequence of different temperature-dependent mechanisms such as population redistribution over different electronic levels (Boltzmann statistics), quenching mechanisms/cross-relaxation, nonradiative decay and phonon-assisted Auger conversion processes [177]. Intensity-based luminescence thermometry (Fig. 10a) enables temperature estimation based on the intensity generated by a single emission band. Higher temperatures increase the probability of nonradiative and quenching pathways, leading to a decrease in absolute intensity and this can be correlated to the tumor temperature. While it is a fast and straightforward method, it is highly affected by NP concentration, illumination intensity and transmission of the surrounding environment, which could lead to wrong absolute readouts. Higher temperatures can, in other materials, induce a shift in the emission wavelength (Fig. 10b) due to electron-phonon interactions. Spectral shift detection usually requires high-resolution measurements and expensive spectral analyzers. Nanothermometry based on emission ratio (Fig. 10c) relies on the relative intensity between different spectral lines. It occurs as a consequence of quenching and nonradiative mechanisms, and the thermal readout is derived from the fluorescence intensity ratio (FIR). FIR is independent of nanothermometer concentration, excitation intensity and photobleaching, making it one of the most reliable temperature sensing methods, and can be applied to materials with single and dual emission centers. Bandwidth luminescence (Fig. 10d) can be achieved by monitoring the width of the emission spectrum lines with the temperature. Higher temperatures often induce a broadening of the emission line, due to phonon-electron coupling. Their application is hence limited to systems exhibiting narrow emission bands. Temperature can also be estimated from the luminescence lifetime of the nanothermometer (Fig. 10e), which represents the time interval required for the emission intensity to decay to $1/e$ of its maximum value, and is related to quenching *via* radiative, nonradiative, and multiphonon mechanisms. Lifetime luminescence often requires rather expensive acquisition systems. Lastly, polarization luminescence thermometry (Fig. 10f) is possible due to the temperature-dependent changes in polarization anisotropy (ratio between luminescence emission intensity at two orthogonal polarization states) [172,177,178]

Over the past couple of decades, numerous fluorescent materials have been developed which display temperature-dependence in the relevant physiological and above-physiological temperature range [172,178]. The choice of nanothermometer should depend on their performance, which is often evaluated based on: thermal sensitivity (S_{abs}/S_{rel}), thermal, spatial and temporal resolution, repeatability, and reproducibility. S_{abs} is expressed in K^{-1} and expresses the degree of change in the thermometric parameter per degree of temperature. S_{rel} is expressed in % K^{-1} and is used to compare the performance of different nanothermometers, expressing the maximum change in thermometric parameter per temperature degree [172]. Nanothermometers for biological applications ideally display strong luminescence, photostability, low toxicity, low photobleaching, excitation and emission wavelengths within the BW, and high stability in biological fluids [172].

Several *in vitro* and *ex vivo* studies have been performed using nanothermometers for temperature mapping. However, *in vivo* testing is still scarce, and mostly limited to QDs and Ln-NPs [176,179,180]. Indeed, the use of nanothermometers as probes for thermal therapies *in vivo* is an extremely novel study area, with only a handful of papers published on the topic (summarized in Table 5). More comprehensive compilations of the *in vitro, in vivo* and *ex vivo* studies using nanothermometry can be found in other review papers by Bednarkiewicz et al. [180] and Zhou et al. [176] In this section, we will focus on briefly explaining the relevance of the most popular nanothermometers and present some of the most relevant results reported so far [179,180].

3.2.1. Fluorescent Proteins

Fluorescent proteins (FPs) can be used as nanothermometers, providing non-invasive and real-time temperature readouts at the intracellular level. Typically, they are used in solution or genetically encoded, by incorporating the genetic sequence in the target cell, forcing it to express the protein. Donner et al. reported the use of a green fluorescent protein (GFP) as an intracellular thermal probe *via* polarization luminescence nanothermometry. HeLa and U-87 MG cells expressing this GFP variant were used to monitor the photoheating of gold nanorods with high thermal (0.4 °C) and spatial (300 nm) resolution [181]. Nakano et al. developed an engineered FP, gTEMP, using Sirius and Mt-Sapphire, two FPs with different thermal sensitivities. This strategy enabled the detection of temperature changes in the cytoplasm, nucleus and mitochondria, in cells and in living medaka embryos, showing temperature monitoring capability both *in vitro* and *in vivo* [182]. While FPs allow for accurate and highly sensitive intracellular temperature detection, they present some drawbacks including time-consuming and highly specialized gene encoding techniques, and measurement errors induced by the surrounding environment [172].

3.2.2. Small Organic Dyes

Organic dyes are commonly used as fluorescent markers in biological applications to tag cell components and monitor metabolic activity. They feature high quantum yields and easy detection. Many of these dyes display thermal sensitivity and can be used as thermal probes. The most relevant examples of small organic nanothermometers are Rhodamine B and fluorescein, as their emission intensity and lifetime are temperature-dependent. Nonetheless, organic dyes present many disadvantages, including limited photostability, high toxicity and the sensitivity of the fluorescence towards pH, polarity and viscosity. Thus, they require careful (re)calibrations in each specific medium, and are prone to environment-induced measurement errors [172,179].

3.2.3. Quantum Dots

Quantum dots (QDs) are fluorescent semiconductor NPs which have been widely explored for biological applications due to their high quantum yields, long lifetime and high stability [172]. In addition, it is possible to tune the discrete electronic states (emission colour) by

Table 5|
In vivo fluorescence nanothermometry studies for temperature mapping in cancer thermal therapies.

Nanothermometer	Λ_{exc} (nm)	Λ_{em} (nm)	Temperature range (°C)	*Srel*(% K^{-1})	Cell Model	Application	Ref.
LaF_3:Nd	808	880	32–53	0.25	Breast cancer xenograft (MDA-MBD-231 cells)	PTT with temperature mapping	[194]
$NaLuF_4$:Yb,Er	980	525/545	20–70	1	Ovarian carcinoma xenograft (HeLa cells)	PTT with temperature mapping	[195]
$NaLuF_4$:Yb,Er	980	525/545	37–46	1	Pancreatic carcinoma	PTT/chemotherapy	[196]
PbS/CdS/ZnS QDs	808	1220	30–67	1	Squamous cell carcinoma xenograft (A431 cells)	PTT with temperature mapping	[197]

changing QD size, shape and chemical composition, which render QDs suitable fluorescent probes [183]. An increase in temperature leads to a decrease in fluorescence intensity as well as a spectral shift, and changes in lifetime, which can be used to correlate the emission spectral data to the temperature changes [184]. For instance, Laha et al. used 2 nm cadmium telluride (CdTe) QDs to measure thermal variations *ex vivo*, having reported a thermal resolution of 1 mK and a spatial resolution of 80 nm [185]. Nonetheless, QDs in biomedical applications have raised concerns related to potential toxicity, due to the presence of heavy metal ions such as lead or cadmium. The development of shelling and functionalization protocols using inert materials is being explored as a way to circumvent QDs toxicity and boost their potential [186]. Other important limitations arise from luminescence variations with the environment, which can lead to errors in thermal sensing [179].

3.2.4. Thermoresponsive Polymers

Polymers are often used as scaffolds to incorporate organic dyes or fluorescent proteins due to their biocompatibility. The incorporation of luminescent monomers within the matrix makes them interesting candidates for thermal sensing. Thermoresponsive polymers undergo reversible phase transition upon temperature changes as a result of the collapse of the polymer chains. This leads to changes in the local luminescent response at a critical transition temperature. Poly(N-isopropylacrylamide) (PNIPAM) is the most popular polymer in nanothermometry, with a transition temperature around 32 °C. Due to the restricted operational temperature range, these polymers have been reported to aid intracellular thermal mapping, detecting thermogenesis by different cell organelles [187]. However, this operation range leads to poor detection capability for thermal ablation temperatures. In addition, fluorophore-incorporated polymers often display low quantum yields, larger sizes and luminescence dependence on other environmental factors besides temperature [172].

3.2.5. Nanodiamonds

The potential of nanodiamonds (NDs) in nanothermometry is attributed to the presence of nitrogen-vacancy centers (NVC). These defects in the normal tetrahedral carbon lattice arise from the combination of a nitrogen atom with a vacant lattice site with two unpaired electrons. In the absence of an external magnetic field and due to spin-spin interactions within the NVC, the energy levels of the ground state triplet can be split into three different sublevels ($m = 0, +1, -1$), a phenomenon known as zero field splitting (ZFS). Changes in temperature influence the spin relaxation rates resulting in variations in the fluorescence spectra. Consequently, temperature sensing using NDs requires the use of optically detected magnetic resonance (ODMR) to manipulate and monitor the spin state, and the acquisition of the fluorescence spectra of the NVC. Fluorescence data can be correlated to temperature using an adequate calibration curve [188,189]. Besides their thermal-sensitivity, NDs are biocompatible and physiochemically inert, and temperature sensing is virtually not affected by pH, viscosity, ion concentration or molecular interactions. The first temperature-sensing report using NDs was delivered by Kucsko et al. in 2013. They showed thermal sensing using NDs introduced in a single human embryonic fibroblast, with high thermal (1.8 mK) sensitivity [190]. Numerous studies have been carried out since then, and are reviewed in detail elsewhere [188,191]. Despite their huge potential, these NPs show a wide size distribution, heterogeneous brightness and low quantum yield, suggesting the need for improved fabrication protocols. Furthermore, their emission is often located in the visible range of the spectra, hindering tissue penetration and thermal image acquisition [172,188].

3.2.6. Lanthanide-doped Nanoparticles

Lanthanide-doped NPs (LN-NPs) display temperature-dependent luminescent properties, with excitation and emission wavelengths within the NIR region for improved penetration depths and temperature readings. Furthermore, Ln-NPs present low phototoxicity and photobleaching. Hence, they have been pointed out as a promising nanothermometer for biological/biomedical applications [172]. These nanomaterials comprise a transparent host, normally a crystalline matrix, that is doped with variable concentrations of one or several Ln^{3+} [179]. The most widely studied lanthanide ions are thulium (Tm^{3+}) and neodymium (Nd^{3+}), mainly due to their emission bands in the 700–800 and 800–950 nm ranges, respectively. Upon laser irradiation, Ln-NPs can also generate heat due to the electronic configuration of Ln^{3+} ions, which leads to radiative and nonradiative mechanisms, promoting luminescence and heat generation, respectively. Thus, Ln-NPs potential as photothermal agents has also been hypothesized. For PTT, Ln-NPs require higher excitation intensities to reach the desired therapeutic temperatures, therefore increasing the risk of phototoxicity [172,192]. Despite their tremendous potential as nanothermometers, there are still some limitations hindering the clinical application of Ln-NPs. For instance, the active ions are often embedded in a nanocrystal structure that requires surface functionalization steps to be stable in aqueous solutions and biocompatible [152].

3.3. Metal Organic Frameworks

Metal organic frameworks (MOFs) have emerged as an interesting candidate for nanothermometry. These consist of a macromolecular crystalline matrix composed of organic-inorganic molecules linked *via* covalent interactions. As a consequence, MOFs display a porous structure, allowing for the insertion of guest fluorescent molecules such as Ln^{3+} ions. This implies the existence of multiple luminescent centers and tunable optical properties by adjusting intermolecular interactions between the frameworks and guest molecules [193]. Besides their tunable luminescence, MOFs also display high thermal sensitivity and resolution. However, they present significant limitations, including low stability in physiological environments and high toxicity, limiting their clinical applications [172].

3.4. Current challenges in luminescent Nanothermometry

While fluorescence nanothermometry is a relatively novel research field, it shows outstanding potential, not least in HT applications. Nanothermometers enable precise, real-time and remote temperature sensing in a 3D biological sample. Notwithstanding this incredibly fast development and potential, nanothermometry still presents some limitations, including the lack of standardized quantitative temperature monitoring techniques and poor knowledge of the thermal response of some materials. This is partly due to limited access to required setups, and experimental complexity due to the multidisciplinary nature of the field [178,179]. Applied to cancer therapies, concerns regarding toxicity, and light scattering and absorbance by biological tissues, have imposed the main limitations to the success of luminescent nanothermometers. However, the development of nanomaterials with tunable excitation and emission in the NIR region has been a successful strategy for nanothermometry. Engineered Ln-NPs with core@shell structures for enhanced signal intensity, and functionalized surfaces for improved biocompatibility, have been reported as the most promising strategy, with several formulations being tested *in vivo* for improved thermal therapies. These NPs allow for great dopant tunability and consequent versatility of operation wavelengths in the different BWs [172,177,179]. Efforts have been made in combining nanothermometers with heat-generating NPs as a dual-function formulation. Alternatively, some research has been carried out to develop a single nanomaterial capable of simultaneously generating heat and monitoring the temperature. LaF_3:Nd NPs, for instance, have been reported to display this dual function when excited at 808 nm. However, the heat generation efficiency is significantly lower than reported for other nanoheaters [194].

As more reliable and optimized nanothermometers are reported, and

imaging capability is improved, more accurate temperature readouts will be achieved. This will allow for a better preclinical characterization of thermal therapies and dosimetry optimization, therefore increasing therapeutic efficiency and reducing toxicity to healthy cells. This could lead to a better clinical translation, speeding their clinical application and commercial use [180].

4. *In vitro* preclinical screening – 3D tumor models

In addition to the challenges of accurate temperature monitoring, achieving a good NP distribution at the tumor site *in vivo* has further hindered the clinical application of NPs as heat mediators. Furthermore, current screening techniques underestimate the role of the tumor microenvironment (TME) components on cell thermotolerance [198]. This section will focus on the use of advanced cancer cell models as platforms for NP screening, for a clinically relevant analysis of therapeutic parameters, NP and heat distribution, and thermotolerance of solid tumors (see Fig. 11) [198].

4.1. NP delivery in vivo

Systemically administered NPs must overcome multiple physiological barriers before reaching the target tumor tissue. These barriers are often overlooked in the preclinical stages of NP testing, leading to poor clinical translatability of nanomedicines [198,199]. The TME comprises both malignant and non-malignant cell types (such as fibroblasts, immune cells, mesenchymal cells and endothelial cells) and the ECM (Fig. 11a). The crosstalk between cellular and acellular components of the TME has been shown to play a determining role in tumor progression, metastasis, and therapeutic response. A major limitation for NP permeability in solid tumors is the existence of differential cellular organization as a result of heterogeneous blood distribution. The peripheral layer of the tumor is often well-vascularized, while there is impaired blood perfusion towards the core. The O_2 and nutrient gradients, together with the accumulation of cellular waste, lead to a hypoxic and acidic core. This prompts the formation of three layers with distinct growth kinetics: the peripheral proliferative layer; the middle non-proliferative, quiescent layer; and the necrotic core [199]. Cell and ECM density gradually increase towards the core, hindering NP diffusion and promoting heterogeneous therapeutic sensitivity [200,201]. NP penetration is further hampered by the presence of the acellular ECM components. The ECM, a dense meshwork of polymers (collagen, fibronectin, glycosaminoglycans, *etc.*), provides structural support to the tumor. During cancer progression, ECM deposition is maximized, significantly increasing the stiffness at the tumor site. This, in turn, promotes the steric restriction of NPs, reducing accumulation at the tumor and ultimately affecting therapeutic outcomes [199]. Additionally, tumor-aiding non-malignant cells also play a role in the efficacy of NP-mediated therapies. For instance, immune cells can trigger inflammation, immune evasion and tumor growth, while promoting off-target NP uptake. Whereas cancer-associated fibroblasts (CAFs) play a crucial role in ECM deposition during tumor progression, contributing to the increased stiffness of the TME [199,202]. In cancer research, designing nanomaterials that circumvent the TME and target tumor cells, effectively relies on the use of biologically relevant preclinical models [199].

4.2. NP preclinical screening

Preclinical NP screening has traditionally relied on two-dimensional (2D) cell culture models and *in vivo* animal models. 2D cell culture

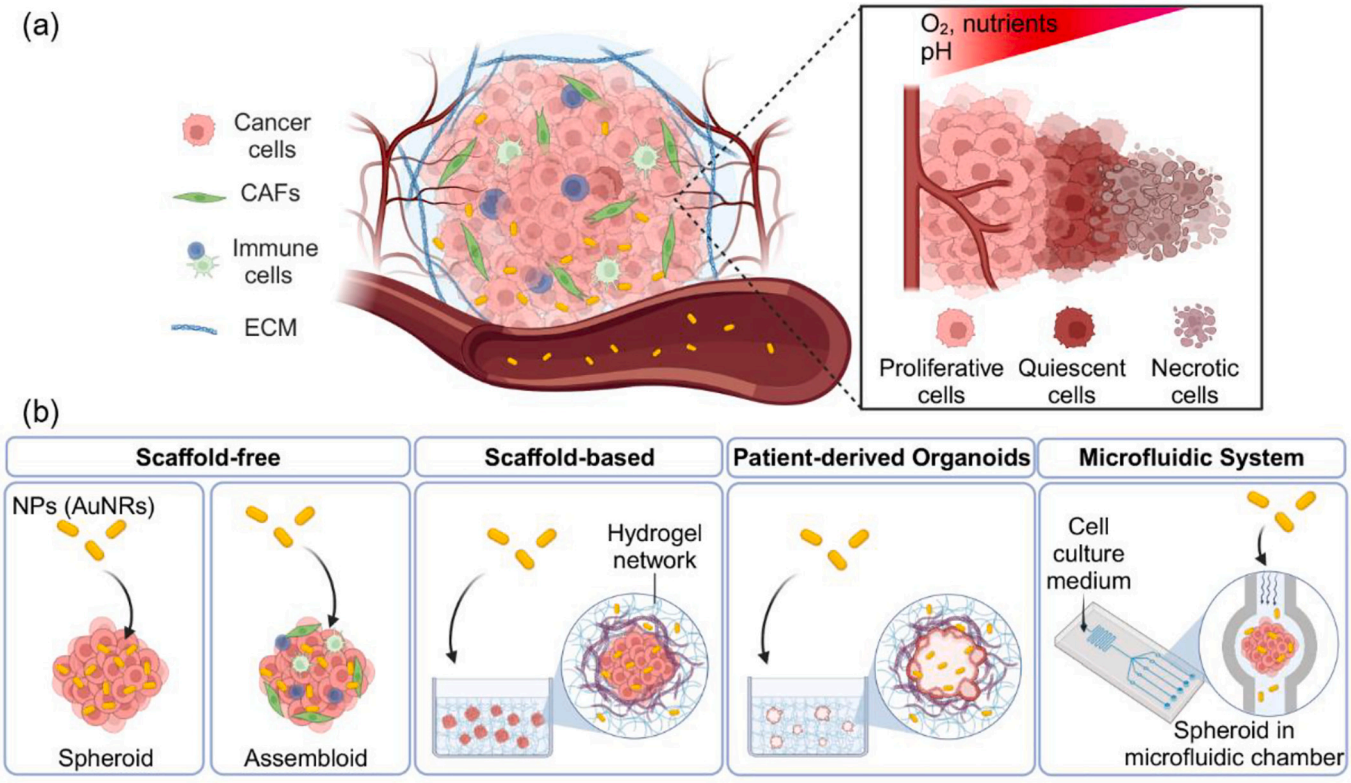

Fig. 11. |(a) Schematic representation of the complex tumor microenvironment (TME) composed of a heterogeneous population of cancer cells and stromal cells (*e.g.*, cancer-associated fibroblasts (CAFs), endothelial cells, and immune cells), and the extracellular matrix (ECM). Tumor growth and progression leads to the formation of distinct cell layers: an external proliferating zone, a middle quiescent zone and an internal necrotic core, as the cells closer to the blood vessels have more access to O_2 and nutrients, creating a gradient within the tumor [228]. (b) 3D tumor models can be designed to mimic different aspects of the TME and predict NP behavior in the body. (Image created with BioRender.com).

systems serve as the primary platform for biological assays and drug screening in cancer research, due to their standardized analytical methods, reproducibility, and cost-effectiveness. Yet, they are overly simplistic in mirroring the physiological conditions of the TME (Fig. 11a) [203,204]. In these systems, cells grow on a flat surface under static conditions, lacking the complex 3D tumor architecture and cell-cell/cell-matrix interactions [199,205]. Furthermore, cells grown on monolayers do not accurately model oxygen, nutrient, and pH gradients that are pivotal in tumor progression and therapeutic resistance [206,207]. Thus, cells in 2D platforms show different heat stress responses compared to solid tumors. Namely, cells in 2D are more prone to cell damage and death in response to NP-HT. Moreover, the distribution of the NPs and heat is very heterogeneous in the TME while the NP distribution and cell damage in monolayer cultures is more homogeneous throughout the population [198]. Despite these limitations, these models offer valuable insight into NP targeting ability, NP uptake by cancer cells and toxicity [199]. Following 2D *in vitro* studies, therapeutic performance is usually validated in *in vivo* platforms as hosts for patient-derived tumor xenografts (PDTX) [208]. Animal models, especially mice, have significantly contributed to bench-to-bedside translation of experimental cancer therapies, serving as tools to understand therapeutic dynamics, including NP pharmacokinetics and biodistribution [209,210]. However, there are fundamental drawbacks to the use of animal systems and PDTXs, including lack of standardization, high variability, and high costs. Underlying differences in biological and physiological processes between the human and murine organisms further affect their applicability [209,210]. Furthermore, animal experimentation is subject to ethical and regulatory concerns, encapsulated in the 3Rs principle (Replacement, Reduction, and Refinement). The 3Rs principle advocates for the use of alternative screening platforms to reduce testing in live animals [211].

The limitations associated with the use of 2D and animal models lead to poor translation from basic research to clinical applications, highlighting the need for novel preclinical tumor models [199]. Recently, 3D cell culture technologies have emerged as a promising link between traditional 2D cell monolayers and clinical trials. The use of 3D cell systems as screening platforms in cancer research can help model the complex physiology of tumors *in vivo*, assisting the design of next-generation NPs with improved tumor accumulation and therapeutic efficacy [212]. These models can reproduce the *in vivo* TME, oxygen/nutrient gradients, and cellular behavior within tumors, including cell proliferation, differentiation and cell-ECM crosstalk [199]. 3D tumor models are also extremely versatile and can be tuned to present different complexity levels. Furthermore, 3D models are more user-friendly, cost-effective and display higher scalability potential than *in vivo* mice models [213]. Regarding HT, cells in 3D models have also been shown to have higher thermo-tolerance, which could be attributed to differential expression levels of heat shock proteins (HSP) [198]. To promote wider application of 3D models in preclinical NP characterization, it is crucial to understand the main features of the different available *in vitro* platforms and their potential in NP-HT research [198].

4.3. 3D tumor models

Over the past decades, several 3D cell culture technologies have been developed with varying features and complexity levels. These include multicellular tumor spheroids (MCTSs) scaffold-free systems, scaffold-based tumor models, patient-derived tumor organoids (PDTOs), and even microfluidic devices (Fig. 11b) [199]. Table 6 provides a comprehensive summary of the advantages, disadvantages, and potential applications of the models discussed in the realm of NP-HT. In the next sections, we will provide a brief overview of the different models currently available for the development of nanomedicines.

4.3.1. Scaffold-free Models

In cancer research, tumor spheroids are the most commonly used 3D systems. This model consists of tumor-mimicking cell aggregates formed by a single cell type or a combination of different cell types, generating a monotypic or heterotypic culture, respectively. During spheroid formation, cells proliferate and secrete their own ECM, establishing stronger interactions and promoting the formation of mature and compact 3D spherical structures (Fig. 11b) [199,215,216]. These models can be used as physiologically relevant tumor models due to their ability

Table 6|
Advantages, disadvantages and potential applications of the available 3D tumor models [108,198,199,214]

Cell Model	Advantages	Disadvantages	Applications in NP-HT Research
Scaffold-free (MCTSs)	• High throughput screening • Low cost and easy manipulation • Mimics solid tumor architecture and physiological and therapeutic gradients • Mimics different cell layers (proliferative, quiescent, and necrotic zones) • Possibility to create co-cultures • Easy imaging and NP tracking	• Lack of cell-ECM interactions • Limited spheroid size • No vascularization	• Evaluate NP penetration depth in solid tumors • Assess targeting ability • Study heat propagation within the tumor mass • Optimize therapeutic parameters (laser/AMF exposure, intensity, etc)
Scaffold-based	• 3D architecture and ECM mimicry • Possibility to tune physical, mechanical and biochemical cues • Allows for single cell or 3D structure seeding • Offers the possibility of co-culture • Relatively easy NP tracking	• No vascularization • High batch-to-batch variability (natural scaffolds) • Harder to harvest samples	• Study cell-ECM interactions and diffusion • Evaluate NP diffusion across the ECM (role of ECM in limiting NP penetration) • Effect of heat on ECM protein degradation • Effect of heat tumors at different stages by tuning scaffold stiffness/composition
Patient-derived organoids	• Patient-specific • Retains parental tumor features • Tissue heterogeneity • High physiological relevance	• No vascularization • Costly • Batch-to-batch variability (natural scaffolds) • Requires specific skills • May require multiple supplements/growth factors	• Personalized medicine • NP-ECM interactions and diffusion • Tumor heterogeneity
Microfluidic devices	• Mimics vascularization • Offers different levels of complexity • Possibility to seed different cell types • High throughput possible • Allows for real-time analysis	• Requires specific skills • Low throughput • Costly	• Comprehensive analysis of NP-TME interactions • Evaluate EPR effect • Study the influence of physiological mimicking flow rates on NP accumulation and therapeutic efficacy

to mimic cell viability, growth kinetics, differentiation, response to stimuli, cell polarization, metabolism, phenotype, and genotype. In spheroids, there are gradients of nutrients, oxygen, and pH, leading to the development of distinct cell proliferation zones, including a proliferative outer layer and a necrotic core. This layered organization reflects the pathophysiological gradients found in *in vivo* tumors (Fig. 11a) [217]. Thus, MCTSs represent the first step to bridge the gap between preclinical and clinical oncology research. In NP research, MCTSs have been used to investigate and optimize NP physicochemical properties, such as NP charge, size, shape, and surface functionalization. In thermal therapies, MCTSs can be used to study heat distribution within the 3D structure and thermal ablation efficiency, facilitating optimization of thermal therapy parameters and NP physicochemical features [199,218].

4.3.2. Scaffold-based Models

While MCTSs can be a valuable tool, these models fall short in fully representing the complex and tumor-specific extracellular matrix (ECM). To address these limitations, biomimetic platforms that model the ECM have gained traction, leading to the evolution of scaffold-based 3D cell culture methods. These methods involve introducing individual cells or cell aggregates into matrices that undergo physical or chemical crosslinking (Fig. 11b) [219]. Different types of scaffolds are used in biomedical research, including natural, synthetic and hybrid materials. Matrigel® is the most widely used scaffold and consists of a decellularized matrix extracted from Engelbreth-Holm-Swarm mouse sarcoma cells, making it a rich source of ECM components, including collagen, laminin and growth factors [220]. Such matrices hold promise as preclinical tumor models, offering a more native-like cellular environment. By taking into account both NP-ECM and NP-cell interactions, these models bring the cell behavior and communication closer to that observed *in vivo* and allow for a closer recapitulation of NP behavior in the body, by contemplating NP-ECM interactions as well as NP-cell interactions [199,204,221].

4.3.3. Patient-derived Tumor Organoids

PDTOs represent another widely described *in vitro* cell model in cancer research. PDTOs closely simulate *in vivo* heterogeneity and TME complexity, including the presence of a cancer stem cell (CSC) population, which greatly influences cancer metastasis and therapeutic resistance (Fig. 11b) [199,222]. PDTOs have been suggested as promising platforms for NP development, as they can effectively mirror patient therapeutic responses, making them valuable for rapid, high-throughput personalized screening. They can also be used to analyze interactions between the ECM, NPs, and cells, and the diffusion and internalization of NPs within the TME. Despite their relevance, to the best of our knowledge, there are no literature reports of NP screening using PDTOs, likely due to their novelty and lack of analysis standardization [199,223].

4.3.4. Microfluidic Devices

Recently, microfluidic-based models, or “organs-on-chips”, have emerged as promising alternatives to traditional culture models due to their ability to replicate physiological conditions and provide valuable insights into drug testing [224,225]. These platforms are dynamic and customizable, featuring microchannels where cells can be cultured under conditions that mimic physiological flows. They can replicate *in vivo* vascular perfusion, 3D cellular architecture, cell-cell/matrix interactions and cellular heterogeneity (Fig. 11b). Microfluidic systems can be used to seed either individual cells or 3D structures like MCTSs, and they enable the inclusion of immune cells, connective tissue cells, and an endothelial lining found in the TME. In nanomedicine, their use can enhance *in vitro-in vivo* correlations, offering insights into toxicity, efficacy, targeting ability, organ accumulation/distribution and real-time NP tracking [224,226,227].

4.4. NP-HT screening using 3D models

Preliminary NP-HT screening using 3D models has proved the antitumor potential of these therapies in advanced 3D systems, while also highlighting the importance of implementing a multifactorial approach for NP optimization. Overall, 3D models help evaluate NP tumor penetration and diffusion through different physiological barriers. They could help characterize the mechanisms of cell death and heat propagation inside the tumor as a function of NP distribution, provide better insights on NP diffusion and accumulation, and facilitate an overall improved NP design for targeted and effective thermoablative therapies. When compared to 2D cultures, 3D cell models can also be maintained for longer times, enabling the study of long-term effects, including recovery and cancer recurrence [108]. Given their advantages, numerous preliminary studies have been performed using 3D tumor models for NP-HT screening. Liu et al. used 3D spheroid models to compare therapeutic efficacy of reduced graphene oxide (rGO)-based chemotherapy (rGO-PEG/DOX), PDT (rGO-PEG/Ce6) and PTT (rGO-PEG) (Fig. 12a). Their results showed that while all three types of therapies displayed high efficacy in 2D monolayer cultures, only PTT showed significant antitumor efficiency in spheroid models, suggesting that heat diffusion in solid tumors is more efficient than the diffusion of therapeutic molecules (Fig. 12b, c). They also observed that thermal ablation was independent of NP penetration in the spheroid. In mice, rGO-based PTT promoted cell apoptosis and vascular damage in tumor tissue, while rGO-based PDT and chemotherapy showed poor treatment efficacy (Fig. 12d). This study highlights the importance of advanced 3D tumor models in providing information that could otherwise not be obtained from oversimplistic 2D tumor models [229]. Crawford et al. used a 3D model for inflammatory breast cancer to replicate tumor emboli. Plasmonic AuNS were introduced for imaging and PTT and thermal ablation was compared in 2D and 3D cell models. Following NP incubation, samples were exposed to an 808 nm continuous wave laser at various laser intensities. In 3D models, the authors showed that the amount of cell death was related to the laser power: while lower laser intensities induced ablation only at the periphery, irradiation with powers above 5 W/cm^2 resulted in cell death across the entire spheroid. Thus, the use of 3D models provided relevant insights into how to tune laser power parameters to achieve successful treatment within the whole solid tumor [230]. Recently, Li et al. designed micelles with various shapes (rod, sphere and worm-shaped) and loaded them with the IR780 PTA. The effect of shape on NP performance was then evaluated for their tumor efficacy against MCF-7 breast cancer cells. Fluorescence data revealed the highest intensity for rod-shaped micelles in both 2D and 3D tumor models. Rod-shaped NPs were then injected in mice xenograft models and irradiated with an 808 nm laser. Tumor temperature after NP activation was 55.6 °C for NP-encapsulated IR780 *vs.* 49 °C for free IR780. This study demonstrated the value of 3D models as a bridge between 2D *in vitro* cultures and *in vivo* models [231]. Preliminary studies have been performed using microfluidic platforms for NP-PTT and NP-MTT [232,233]. For instance, Mamani et al. evaluated the effectiveness of NP-MTT on a glioblastoma model using an organ-on-a-chip. Murine glioma C6 cells were cultured in a microfluidic device and exposed to aminosilane-coated MNPs under an AMF. The results showed complete cell lysis after 30 min of AMF exposure, demonstrating the potential of MTT in treating glioblastoma using a biologically relevant tumor model [233]. This research highlights the significance of microfluidic-based models in advancing nanomedicine and potentially minimizing the need for animal testing, thereby accelerating therapeutic development [224]. A comprehensive compilation of the available publications can be found in Table 7.

Advanced 3D *in vitro* tumor models have been used in the screening of numerous formulations for NP-PTT, NP-MTT and combination therapies. These studies have confirmed the ability of NPs to promote local hyperthermia in solid tumors, and highlighted the importance of considering the complex TME and adopting an integrative multi-omics

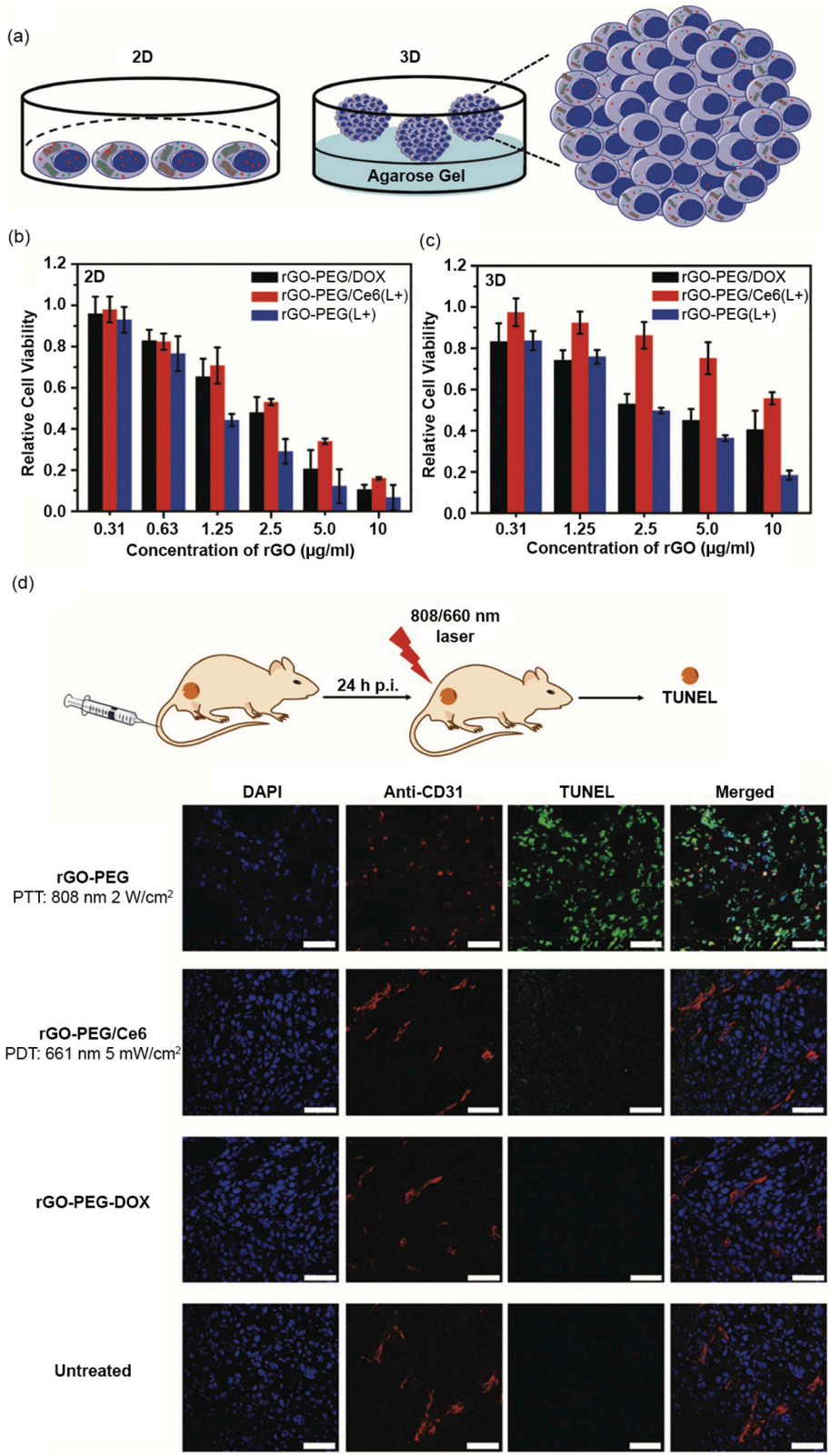

Fig. 12. (a) Anti-tumor performance of reduced graphene oxide (rGO) was evaluated in 2D and 3D *in vitro* tumor models. AuNSs are endocytosed by tumor emboli spheroid models. The therapeutic efficacy of three rGO-based treatment modalities (NP-mediated chemotherapy, NP-PDT and NP-PTT) were assessed *via* cell viability assays in (b) 2D tumor monolayers (MTT assay) and (c) 3D tumor spheroids (APH assay). Results showed higher PTT efficacy compared with chemotherapy and PDT in both 2D and 3D. (d) Fluorescence images of tumor slices from *in vivo* mouse models. Apoptosis detection was achieved using the TUNEL assay of tumors from three rGO-based treatment groups and untreated group. Blue, red and green represent DAPI stained cell nuclei, anti-CD31 antibody-stained blood vessels and apoptosis labeling (TUNEL) channels, respectively. The scale bar is 50 μm. Reprinted from [229]. (For interpretation of the references to colour in this figure legend, the reader is referred to the web version of this article.)

Table 7|
Comprehensive overview of recent studies using advanced 3D *in vitro* tumor models as platforms for NP-HT screening.

Type of MNP		Size (nm)	Coating	Cancer type	Tumor Model	Application	Reference
NP-PTT	AuNR	55 × 14	PDDAC, CTAB, PSS	Breast cancer	3D spheroid	Influence of NP charge on tissue penetration for PTT	[234]
	AuNP	18.4	PEG	Colorectal cancer	3D spheroid	Influence of synergistic PTT + CT on drug resistant cancer therapy	[235]
	AuNS	50	–	Inflammatory breast cancer	3D spheroid	PTT potential in 2D *vs* 3D models	[230]
	IR-DOX/BSA	92.3	SBMA	Breast cancer	3D spheroid	Influence of PTT + CT synergistic potential	[236]
	$Ti_3C_2T_X$ nanosheets	2 μm length	–	Murine Breast cancer	3D spheroid and bioprinted hydrogel-embedded cancer cells	Effect of PTT on advanced 3D cell models	[212]
	rGO@C6/DOX	50–150	PEG	Glioma	3D spheroid	Therapeutic efficacy of PTT, CT and PDT on 2D *vs* 3D tumor models	[229]
	PDA-ICG-DOX	328	–	Breast cancer	3D spheroid	PTT-CT potential	[237]
	TMC/PdNPs	70		Breast cancer	3D spheroid	Compare PTT in 2D *vs* 3D tumor models	[238]
	AuNPs-Cis	112	Silica	Neck squamous carcinoma	3D spheroid	Synergistic PTT-CT effect	[239]
	Au nanoarchitectures	124.3	Silica	Pancreatic adenocarcinoma	3D spheroid	PTT efficiency in 2D *vs* 3D	[240]
	Fe_3O_4@Au Core-shell	142	–	Glioblastoma	3D spheroid	Imaging-guided focused PTT	[241]
	CND-P	7–10	–	Breast cancer	3D aggregate	2P PTT in 3D models	[242]
	SWNH	–	–	Breast cancer	Hydrogel-embedded cancer cells	Quantitatively assess 3D viability in response to PTT	[243]
	AuNPs	25	Ker	Glioblastoma	3D bioprinted model	PTT potential in 3D tumor model	[244]
	HGNs	–	Anti-MUC1	Breast and lung cancer	Microfluidic platform	PTT potential under dynamic administration	[232]
NP-MTT	IONP10	10	–	Breast cancer	3D spheroid	MTT potential of inhalable composites containing MNPs	[245]
	FluidMAG/C11-D	83	–	Pancreatic cancer	3D assembloids (cancer cell co-cultures with fibroblast)	Effect of mild HT on heterotypic 3D spheroids	[246]
	Fe_3O_4	100	Aminosilane	Murine Glioblastoma	Microfluidic platform	MTT potential of MNPs under dynamic administration	[233]

Abbreviations: AuNR – Gold nanorod; PDDAC - Poly(diallyldimethylammonium chloride; CTAB - Cetyltrimethylammonium bromide; PSS - Polystyrene sulfonate; PEG – Polyethylene glycol; AuNS – Gold nanostar; IR – Indocyanine green (PTT agent); DOX – Doxorubicin; BSA – Bovine serum albumin; SBMA – Sulfobetaine methacrylate; $Ti_3C_2T_X$ nanosheets – Bioactive nanomaterials for PTT; rGO – Reduced graphene oxide; PDT – Photodynamic therapy; TMC – Trimethyl chitosan; Pd – Palladium; Cis – Cisplatin; CND-P – Passivated carbon nanohybrid dots; 2P - Two-photon; SWNH – Single-walled nanohorn; Ker – Keratine; HGN – Hollow gold nanoshells; Anti-MUC1 – Anti-Mucin1 aptamer; FluidMAG/C11-D – Commercial IONPs.

approach to study NP suitability for clinical applications [108]. The use of physiologically relevant screening models would enable a more thorough evaluation of heat diffusion within a solid tumor. It would also allow for a careful NP design and therapeutic parameter optimization for adjuvant hyperthermia *vs* thermal ablation (low power density and high exposure time *vs.* high power density and low exposure time). Moreover, heat generation and NP diffusion and permeability as a function of NP physicochemical properties (material, size, charge, shape and surface functionalization), could be thoroughly understood and modulated in the preclinical setting. The possibility to incubate and study 3D culture models for longer periods paves the way for the short and long-term characterization of these therapies, including cell death mechanisms, the role of the TME on heat resistance, cancer recovery and heat shock protein production. Lastly, NP-TME crosstalk can be studied, improving the understanding of the ECM and stromal influence on NP performance, as well as the impact of NP-HT on the TME [108,198,199]. This knowledge could boost the design of safe and efficient nanomaterials with improved performances for safe clinical applications in cancer therapy. While 3D tumor models have been shown to be promising *in vitro* methods to mimic the features of most solid tumors, they are still far from being used as the gold standard for preclinical studies in nanomedicine research. In addition, further optimization is required to achieve an accurate correlation between 3D models and *in vivo* NP behavior, internalization and therapeutic efficacy. These include the lack of standardized sample preparation, characterization, imaging, quantification and analysis protocols. Nonetheless, impressive advances in microscopy techniques, including multi-photon laser scanning microscopy and light-sheet microscopy, set the scene for better established methods for NP design and optimization using 3D preclinical models. Such progress may be the key to boosting the implementation of these 3D culture systems in preclinical oncology and to closing the current translational gap that hinders the development of improved nano-based cancer therapies [199].

4.5. *Temperature monitoring in advanced 3D tumor models*

NP-HT has demonstrated potential in *in vitro* studies and numerous clinical human trials. However, the uncontrolled NP distribution within

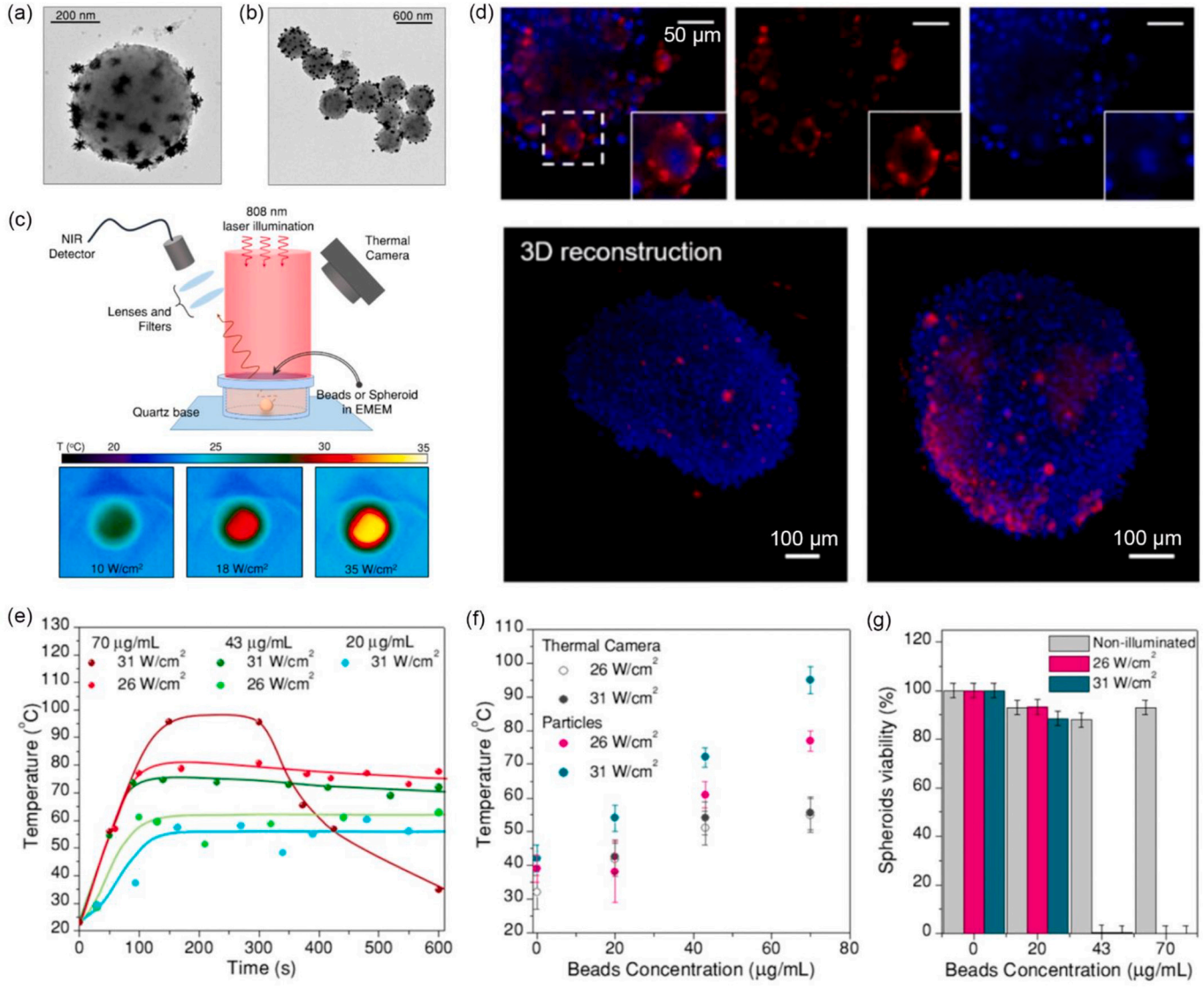

Fig. 13|. (a) TEM images of assembled beads before silica coating and (b) after silica coating; (c) Experimental set-up used to excite the samples (808 nm) and recorded luminescence and temperature using an NIR detector and a thermal camera; (d) Fluorescence images of the spheroids showing untreated and treated spheroids (150 µg/mL): Nd^{3+} emission (red channel) is apparently located in the cytoplasm, as the blue channel stands for the DAPI staining of the cell nuclei. (e) Temperature measurements inside spheroids during PTT: thermal evolution over time for different excitation powers and bead concentration; (f) Average temperature at thermal equilibrium for each treatment, compared to the thermal camera readouts; (g) Spheroid viability at 24 h after PTT. Reprinted from [248].

the tumor and the complexity of the TME, make it challenging to achieve accurate control of the therapeutic temperature. As a result, these therapies still require validation to facilitate their use in the clinic [247,248]. The combined application of adequate temperature-monitoring techniques with advanced *in vitro* 3D tumor models could enable a thorough study of NP performance and a careful optimization of therapeutic parameters. Due to the tumor-like features of 3D *in vitro* models, this preclinical strategy could significantly improve bench-to-bedside translation, paving the way for the design of nanomaterials with higher anti-cancer potential and enhanced clinical translation, which could boost NP-HT application in oncology research (see Fig. 13) [99].

The combination of nanothermometry and advanced 3D models in NP screening is a novel strategy. To the best of our knowledge, only one study has been published reporting this approach for cancer hyperthermia. Quintanilla et al. (2019) developed a silica-coated hybrid nanostructure (~500 nm) that combined plasmonic AuNSs with CaF_2:Nd^{3+},Y^{3+} nanothermometers (Fig. 13a, b). They tested the emission and heating properties using a NIR detector and a thermal camera, adjusting illumination parameters to control temperatures between 37 °C and 100 °C for PTT (Fig. 13c). The permeability and PTT efficacy of the NPs were tested in glioblastoma spheroids. NP tracking within the 3D model was achieved using a Light Sheet microscope (Fig. 13d), demonstrating the NP's ability to penetrate deep into the spheroid mass. This study showed PTT-induced cell death in tumor spheroids while allowing for *in situ* temperature readouts (Fig. 13e, f). The authors also highlighted the need to improve bead size and the number of nanothermometers per AuNS for enhanced luminescence and time resolution in 3D cell models [248]. This information provides valuable insights into the innovative use of nanothermometry and advanced 3D models in NP screening, supporting the potential of this approach for improving the understanding of NP behavior and its application in cancer treatment.

5. Summary and future prospects

NP-mediated thermal cancer therapies, namely PTT and MTT, have shown great potential for noninvasive and selective cancer treatment. Over the past decades, tremendous breakthroughs in the field of nanomedicine have led to the development of a wide range of nanomaterials with heating capabilities. In particular, research has been focusing on the development of NPs for PTT and MTT applications. Among the most widely studied NPs for cancer thermal therapies are AuNPs and IONPs, for heat generation upon NIR light irradiation and AMF excitation, respectively [44,98]. These materials are extremely versatile and can be finely tuned for optimal heat generation and tumor internalization, and several comprehensive reports can be found on the effect of different characteristics on NP performance. However, most studies are performed in 2D *in vitro* cell models, and promising results often cannot be replicated *in vivo*. In the body, therapeutic action is hindered by inadequate NP and heat distribution inside the tumor, and more robust preclinical techniques are needed to improve clinical translation of NP-HT [13,199]. This review identifies two main gaps in preclinical screening: the lack of accurate real-time temperature monitoring techniques and the lack of adequate tumor models to evaluate NP performance. To address these challenges and propose innovative strategies, this review serves as a comprehensive guide for researchers and practitioners in the field, offering insights into the latest developments in NPs for HT applications, nanothermometry and advanced tumor models. By exploring the synergistic potential of the last two fields, we aim to boost NP-HT development and application, ultimately contributing to the advancement of cancer treatment modalities. Over the past 5 years, some studies have suggested the combination of nanothermometric strategies and advanced tumor models as a comprehensive and robust preclinical analysis of NP-HT. By combining the temperature-monitoring potential of luminescent nanothermometers and the tumor-like features of 3D cancer platforms, it is possible to predict the behavior of these therapies more accurately in solid tumors in the human body, significantly increasing clinical translatability and application of these materials [248].

While the combination of accurate real-time temperature monitoring techniques and biologically relevant 3D *in vitro* models poses an extremely promising avenue for higher clinical application of NP-HT, both areas of research are relatively recent. Hence, further advancements are yet to be made to establish them as standard tools in NP design and characterization within preclinical settings. Luminescent nanothermometers have been suggested as one of the most promising probes for remote, real-time temperature monitoring. However, concerns remain regarding the limited light penetration depth, and thermal resolution, as well as low emission intensity in the NIR biological transparency windows, leading to potential inaccuracies in thermal readouts. Recently developed lanthanide-doped nanocrystals have shown improved temperature-dependent performance in the NIR range, although issues with stability in biological environments persist. To overcome this drawback, encapsulation and functionalization strategies offer promising solutions to protect thermal probes from the environment, therefore improving stability. The development of easy-to-use experimental setups for NIR region could facilitate the integration of nanothermometry in biological and clinical settings. The wider application of nanothermometers could also be accelerated by using biologically relevant characterization models [178,179].

3D *in vitro* tumor models have emerged as valuable screening platforms for NPs, mirroring key aspects of *in vivo* tumors. Despite their potential, their use is not yet standard practice. One of the main limitations is the complexity of preparation methods and characterization assays, in comparison to 2D models. For instance, the application of standard confocal microscopy is often insufficient, and more advanced microscopy techniques are needed. Nonetheless, significant advances have been made in microscopy and cell culture techniques, paving the way for the establishment of 3D models as preclinical models in NP-HT design. This could help close the current knowledge gap regarding the influence of tumor physiology on NP performance, as well as the effect of NP physicochemical properties (*i.e.* charge, shape, size) on HT ability and therapeutic efficiency. Therefore, the use of standardized 3D tumor models poses a crucial step to understand NP stability, biocompatibility, toxicity, and targeting ability in biological environments. More importantly, in combination with temperature monitoring techniques, these advanced preclinical tumor models could predict clinical outcomes, including safety and therapeutic efficacy. This would promote the design of optimized nanomaterials for NP-HT with enhanced performance, contributing to clinical application [199]. To the best of our knowledge, no review has been published covering the synergistic potential of nanothermometers and 3D models in assessing the anti-cancer potential of nanoheaters. This review aims to emphasize the importance of interdisciplinary research in improving bench-to-bedside translation of nanomaterials in cancer hyperthermia and boost the design of optimized materials to be used in the clinic.

CRediT authorship contribution statement

M. Bravo: Writing – review & editing, Writing – original draft, Project administration, Formal analysis, Conceptualization. **B. Fortuni:** Writing – review & editing, Supervision, Formal analysis. **P. Mulvaney:** Writing – review & editing, Supervision, Project administration, Funding acquisition. **J. Hofkens:** Writing – review & editing, Supervision, Project administration, Funding acquisition. **H. Uji-i:** Writing – review & editing, Supervision, Project administration, Funding acquisition. **S. Rocha:** Writing – review & editing, Supervision, Project administration, Methodology, Formal analysis, Conceptualization. **J.A. Hutchison:** Writing – review & editing, Supervision, Project administration, Methodology, Formal analysis, Conceptualization.

Declaration of competing interest

None.

Data availability

The raw data required to reproduce the findings discussed in this review may be obtainable from the primary sources.

Acknowledgements

The authors are thankful to the Global PhD partnership program between KU Leuven and Melbourne University (GPUM/21/025). MB, PM, and JAH thank the Australian Government for funding through the Australian Research Council (ARC) Centre of Excellence in Exciton Science (CE170100026). JAH acknowledges award of an ARC Future Fellowship (FT180100295). JH, HU, BF and SR acknowledged the financial support from Research Foundation of Flanders (FWO) research grants (G0D4519N, G081916N, VS08523N, G0C1821N), postdoctoral fellowship (for BF, 12X1419N and 12X1423N), and from the KU Leuven (C14/15/053, C14/19/079, C14/22/085). J.H. acknowledges support of the Max Planck Institute (MPI) as a fellow.

References

[1] S.K. Sriraman, B. Aryasomayajula, V.P. Torchilin, Barriers to drug delivery in solid tumors, Tissue Barriers 2 (2014) e29528.
[2] L. Yang, et al., Targeting cancer stem cell pathways for cancer therapy, Sig Transduct Target Ther 5 (2020) 8.
[3] D. Hanahan, R.A. Weinberg, Hallmarks of Cancer: the next generation, Cell 144 (2011) 646–674.
[4] J. Beik, et al., Nanotechnology in hyperthermia cancer therapy: from fundamental principles to advanced applications, J. Control. Release 235 (2016) 205–221.
[5] H.P. Kok, et al., Heating technology for malignant tumors: a review, Int. J. Hyperth. 37 (2020) 711–741.
[6] P. Kaur, M.L. Aliru, A.S. Chadha, A. Asea, S. Krishnan, Hyperthermia using nanoparticles – promises and pitfalls, Int. J. Hyperth. 32 (2016) 76–88.
[7] S. Fernandes, et al., Magnetic nanoparticle-based hyperthermia mediates drug delivery and impairs the tumorigenic capacity of quiescent colorectal Cancer stem cells, ACS Appl. Mater. Interfaces 13 (2021) 15959–15972.
[8] M. Khafaji, M. Zamani, M. Golizadeh, O. Bavi, Inorganic nanomaterials for chemo/photothermal therapy: a promising horizon on effective cancer treatment, Biophys. Rev. 11 (2019) 335–352.
[9] G. Hannon, F.L. Tansi, I. Hilger, A. Prina-Mello, The effects of localized heat on the hallmarks of Cancer, Adv. Therap. 4 (2021) 2000267.
[10] Z. Behrouzkia, Z. Joveini, B. Keshavarzi, N. Eyvazzadeh, R.Z. Aghdam, Hyperthermia: how can it be used? Oman Med. J. 31 (2016) 89–97.
[11] P.R. Stauffer, S.N. Goldberg, Introduction: thermal ablation therapy, Int. J. Hyperth. 20 (2004) 671–677.
[12] A. Rajan, N.K. Sahu, Review on magnetic nanoparticle-mediated hyperthermia for cancer therapy, J. Nanopart. Res. 22 (2020) 319.
[13] D.K. Chatterjee, P. Diagaradjane, S. Krishnan, Nanoparticle-mediated hyperthermia in cancer therapy, Ther. Deliv. 2 (2011) 1001–1014.
[14] K. Graham, E. Unger, Overcoming tumor hypoxia as a barrier to radiotherapy, chemotherapy and immunotherapy in cancer treatment, IJN 13 (2018) 6049–6058.
[15] P. Elming, et al., Hyperthermia: the optimal treatment to overcome radiation resistant hypoxia, Cancers 11 (2019) 60.
[16] D.C. Phung, et al., Combined hyperthermia and chemotherapy as a synergistic anticancer treatment, J. Pharm. Investig. 49 (2019) 519–526.
[17] Z.R. Stephen, M. Zhang, Recent Progress in the synergistic combination of nanoparticle-mediated hyperthermia and immunotherapy for treatment of Cancer, Adv Healthcare Materials 10 (2021) 2001415.
[18] S. Kumari, N. Sharma, S.V. Sahi, Advances in Cancer therapeutics: conventional thermal therapy to nanotechnology-based Photothermal therapy, Pharmaceutics 13 (2021) 1174.
[19] G.Y. Yi, M.J. Kim, H.I. Kim, J. Park, S.H. Baek, Hyperthermia treatment as a promising anti-Cancer strategy: therapeutic targets, perspective mechanisms and synergistic combinations in experimental approaches, Antioxidants 11 (2022) 625.
[20] A. Abbasi Kajani, S. Haghjooy Javanmard, M. Asadnia, A. Razmjou, Recent advances in nanomaterials development for nanomedicine and Cancer, ACS Appl. Bio Mater. 4 (2021) 5908–5925.
[21] C.F. Adhipandito, S.-H. Cheung, Y.-H. Lin, S.-H. Wu, Atypical renal clearance of nanoparticles larger than the kidney filtration threshold, IJMS 22 (2021) 11182.
[22] T. Sun, et al., Engineered nanoparticles for drug delivery in Cancer therapy, Angew. Chem. Int. Ed. (2014), https://doi.org/10.1002/anie.201403036 n/a-n/a.
[23] M. Karakotchian, I.S. Fraser, An ultrastructural study of microvascular inter-endothelial tight junctions in normal endometrium, Micron 38 (2007) 632–636.
[24] S. Wilhelm, et al., Analysis of nanoparticle delivery to tumours, Nat. Rev. Mater. 1 (2016) 16014.
[25] U. Ruman, S. Fakurazi, M.J. Masarudin, M.Z. Hussein, Nanocarrier-based therapeutics and Theranostics drug delivery Systems for Next Generation of liver Cancer Nanodrug modalities, IJN 15 (2020) 1437–1456.
[26] B. Bahrami, et al., Nanoparticles and targeted drug delivery in cancer therapy, Immunol. Lett. 190 (2017) 64–83.
[27] Y. Barenholz, (Chezy)., Doxil® — the first FDA-approved nano-drug: lessons learned, J. Control. Release 160 (2012) 117–134.
[28] A. Wicki, D. Witzigmann, V. Balasubramanian, J. Huwyler, Nanomedicine in cancer therapy: challenges, opportunities, and clinical applications, J. Control. Release 200 (2015) 138–157.
[29] V.-M. Bala, et al., Nanoparticle-mediated hyperthermia and cytotoxicity mechanisms in Cancer, IJMS 25 (2023) 296.
[30] L. Yao, D. Bojic, M. Liu, Applications and safety of gold nanoparticles as therapeutic devices in clinical trials, J Pharmaceutical Analysis 13 (2023) 960–967.
[31] J.F. Soeiro, et al., Advances in screening hyperthermic nanomedicines in 3D tumor models, Nanoscale Horiz. (2024), https://doi.org/10.1039/D3NH00305A, 10.1039.D3NH00305A.
[32] FDA approves DaunoXome as first-line therapy for Kaposi's sarcoma. Food and Drug Administration, J. Int. Assoc. Phys. AIDS Care 2 (1996) 50–51.
[33] M.S. Angst, D.R. Drover, Pharmacology of drugs formulated with DepoFoam???: A sustained release drug delivery system for parenteral administration using multivesicular liposome technology, Clin. Pharmacokinet. 45 (2006) 1153–1176.
[34] G. Batist, J. Barton, P. Chaikin, C. Swenson, L. Welles, Myocet (liposome-encapsulated doxorubicin citrate): a new approach in breast cancer therapy, Expert. Opin. Pharmacother. 3 (2002) 1739–1751.
[35] D. Bobo, K.J. Robinson, J. Islam, K.J. Thurecht, S.R. Corrie, Nanoparticle-based medicines: A review of FDA-approved materials and clinical trials to date, Pharm. Res. 33 (2016) 2373–2387.
[36] C.M. Dawidczyk, et al., State-of-the-art in design rules for drug delivery platforms: lessons learned from FDA-approved nanomedicines, J. Control. Release 187 (2014) 133–144.
[37] P.A. Dinndorf, J. Gootenberg, M.H. Cohen, P. Keegan, R. Pazdur, FDA drug approval summary: Pegaspargase (Oncaspar®) for the first-line treatment of children with acute lymphoblastic leukemia (ALL), Oncologist 12 (2007) 991–998.
[38] J.E. Frampton, Mifamurtide: A review of its use in the treatment of osteosarcoma, Pediatr. Drugs 12 (2010) 141–153.
[39] M. Zhao, D. van Straten, M.L.D. Broekman, V. Préat, R.M. Schiffelers, Nanocarrier-based drug combination therapy for glioblastoma, Theranostics 10 (2020) 1355–1372.
[40] F. Rodríguez, et al., Nano-based approved Pharmaceuticals for Cancer Treatment: present and future challenges, Biomolecules 12 (2022) 784.
[41] L. Zeng, et al., Advancements in nanoparticle-based treatment approaches for skin cancer therapy, Mol. Cancer 22 (2023) 10.
[42] Z. Ashikbayeva, et al., Application of nanoparticles and nanomaterials in thermal ablation therapy of Cancer, Nanomaterials 9 (2019) 1195.
[43] R.L. Manthe, S.P. Foy, N. Krishnamurthy, B. Sharma, V. Labhasetwar, Tumor ablation and nanotechnology, Mol. Pharm. 7 (2010) 1880–1898.
[44] P. Das, M. Colombo, D. Prosperi, Recent advances in magnetic fluid hyperthermia for cancer therapy, Colloids Surf. B: Biointerfaces 174 (2019) 42–55.
[45] R.K. Gilchrist, et al., Selective inductive heating of lymph nodes, Ann. Surg. 146 (1957) 596–606.
[46] M. Colombo, et al., Biological applications of magnetic nanoparticles, Chem. Soc. Rev. 41 (2012) 4306.
[47] A. Farzin, S.A. Etesami, J. Quint, A. Memic, A. Tamayol, Magnetic nanoparticles in Cancer therapy and diagnosis, Adv. Healthc. Mater. 9 (2020) 1901058.
[48] K. Maier-Hauff, et al., Efficacy and safety of intratumoral thermotherapy using magnetic iron-oxide nanoparticles combined with external beam radiotherapy on patients with recurrent glioblastoma multiforme, J. Neuro-Oncol. 103 (2011) 317–324.
[49] Q.A. Pankhurst, J. Connolly, S.K. Jones, J. Dobson, Applications of magnetic nanoparticles in biomedicine, J. Phys. D. Appl. Phys. 36 (2003) R167–R181.
[50] M. Xing, et al., Iron-based magnetic nanoparticles for multimodal hyperthermia heating, J. Alloys Compd. 871 (2021) 159475.
[51] X. Yu, R. Yang, C. Wu, B. Liu, W. Zhang, The heating efficiency of magnetic nanoparticles under an alternating magnetic field, Sci. Rep. 12 (2022) 16055.
[52] A.V. Samrot, C.S. Sahithya, A.J. Selvarani, S.K. Purayil, P. Ponnaiah, A review on synthesis, characterization and potential biological applications of superparamagnetic iron oxide nanoparticles, Current Research in Green and Sustainable Chemistry 4 (2021) 100042.
[53] V.V. Mody, A. Singh, B. Wesley, Basics of magnetic nanoparticles for their application in the field of magnetic fluid hyperthermia, European J Nanomed 5 (2013).
[54] K.D. Bakoglidis, K. Simeonidis, D. Sakellari, G. Stefanou, M. Angelakeris, Size-dependent mechanisms in AC magnetic hyperthermia response of Iron-oxide nanoparticles, IEEE Trans. Magn. 48 (2012) 1320–1323.

[55] P. Ilg, M. Kröger, Dynamics of interacting magnetic nanoparticles: effective behavior from competition between Brownian and Néel relaxation, Phys. Chem. Chem. Phys. 22 (2020) 22244–22259.
[56] X. Liu, et al., Comprehensive understanding of magnetic hyperthermia for improving antitumor therapeutic efficacy, Theranostics 10 (2020) 3793–3815.
[57] S.K. Sharma, N. Shrivastava, F. Rossi, L.D. Tung, N.T.K. Thanh, Nanoparticles-based magnetic and photo induced hyperthermia for cancer treatment, Nano Today 29 (2019) 100795.
[58] R.V. Stigliano, et al., Mitigation of eddy current heating during magnetic nanoparticle hyperthermia therapy, Int. J. Hyperth. 32 (2016) 735–748.
[59] R. Chen, M.G. Christiansen, P. Anikeeva, Maximizing hysteretic losses in magnetic ferrite nanoparticles *via* model-driven synthesis and materials optimization, ACS Nano 7 (2013) 8990–9000.
[60] W.J. Atkinson, I.A. Brezovich, D.P. Chakraborty, Usable frequencies in hyperthermia with thermal seeds, IEEE Trans. Biomed. Eng. BME-31 (1984) 70–75.
[61] I.A. Brezovich, R.F. Meredith, Practical aspects of ferromagnetic thermoseed hyperthermia, Radiol. Clin. North Am. 27 (1989) 589–602.
[62] B. Herrero de la Parte, et al., Proposal of new safety limits for in vivo experiments of magnetic hyperthermia antitumor therapy, Cancers 14 (2022) 3084.
[63] C. Pucci, Degl'Innocenti, A., Belenli Gümüş, M. & Ciofani, G., Superparamagnetic iron oxide nanoparticles for magnetic hyperthermia: recent advancements, molecular effects, and future directions in the omics era, Biomater. Sci. 10 (2022) 2103–2121.
[64] S. Khizar, et al., Magnetic nanoparticles: multifunctional tool for cancer therapy, Expert Opin. Drug Deliv. 20 (2023) 189–204.
[65] J.K. Kang, et al., Principles and applications of nanomaterial-based hyperthermia in cancer therapy, Arch. Pharm. Res. 43 (2020) 46–57.
[66] A. Hervault, N.T.K. Thanh, Magnetic nanoparticle-based therapeutic agents for thermo-chemotherapy treatment of cancer, Nanoscale 6 (2014) 11553–11573.
[67] H. Fatima, T. Charinpanitkul, K.-S. Kim, Fundamentals to apply magnetic nanoparticles for hyperthermia therapy, Nanomaterials 11 (2021) 1203.
[68] W. Xie, et al., Shape-, size- and structure-controlled synthesis and biocompatibility of iron oxide nanoparticles for magnetic theranostics, Theranostics 8 (2018) 3284–3307.
[69] T. Vangijzegem, et al., Superparamagnetic Iron oxide nanoparticles (SPION): from fundamentals to state-of-the-art innovative applications for Cancer therapy, Pharmaceutics 15 (2023) 236.
[70] A. Demortière, et al., Size-dependent properties of magnetic iron oxidenanocrystals, Nanoscale 3 (2011) 225–232.
[71] E. Wetterskog, et al., Precise control over shape and size of iron oxide nanocrystals suitable for assembly into ordered particle arrays, Sci. Technol. Adv. Mater. 15 (2014) 055010.
[72] Z. Zhou, et al., Anisotropic shaped Iron oxide nanostructures: controlled synthesis and proton relaxation shortening effects, Chem. Mater. 27 (2015) 3505–3515.
[73] X.L. Liu, et al., Optimization of surface coating on Fe3O4 nanoparticles for high performance magnetic hyperthermia agents, J. Mater. Chem. 22 (2012) 8235.
[74] P.-E. Le Renard, et al., Magnetic and in vitro heating properties of implants formed in situ from injectable formulations and containing superparamagnetic iron oxide nanoparticles (SPIONs) embedded in silica microparticles for magnetically induced local hyperthermia, J. Magn. Magn. Mater. 323 (2011) 1054–1063.
[75] M.F. Attia, N. Anton, J. Wallyn, Z. Omran, T.F. Vandamme, An overview of active and passive targeting strategies to improve the nanocarriers efficiency to tumour sites, J. Pharm. Pharmacol. 71 (2019) 1185–1198.
[76] M. Soleymani, et al., Effects of multiple injections on the efficacy and cytotoxicity of folate-targeted magnetite nanoparticles as theranostic agents for MRI detection and magnetic hyperthermia therapy of tumor cells, Sci. Rep. 10 (2020) 1695.
[77] X.L. Liu, et al., Magnetic Vortex Nanorings: A new class of hyperthermia agent for highly efficient in vivo regression of tumors, Adv. Mater. 27 (2015) 1939–1944.
[78] P. Guardia, et al., Water-soluble Iron oxide Nanocubes with high values of specific absorption rate for Cancer cell hyperthermia treatment, ACS Nano 6 (2012) 3080–3091.
[79] Y. Qu, et al., Enhanced synergism of thermo-chemotherapy by combining highly efficient magnetic hyperthermia with magnetothermally-facilitated drug release, Nanoscale 6 (2014) 12408–12413.
[80] H. Gao, et al., Ellipsoidal magnetite nanoparticles: a new member of the magnetic-vortex nanoparticles family for efficient magnetic hyperthermia, J. Mater. Chem. B 8 (2020) 515–522.
[81] Qu, Y. *et al.* Enhanced Magnetic Fluid Hyperthermia by Micellar Magnetic Nanoclusters Composed of $Mn_xZn_{1-x}Fe_2O_4$ Nanoparticles for Induced Tumor Cell Apoptosis. ACS Appl. Mater. Interfaces 6, 16867–16879 (2014).
[82] H. Wu, et al., Injectable thermosensitive magnetic nanoemulsion hydrogel for multimodal-imaging-guided accurate thermoablative cancer therapy, Nanoscale 9 (2017) 16175–16182.
[83] X.L. Liu, et al., Synthesis of ferromagnetic $Fe_{0.6}Mn_{0.4}O$ Nanoflowers as a new class of magnetic Theranostic platform for in vivo T_1 -T_2 dual-mode magnetic resonance imaging and magnetic hyperthermia therapy, Adv. Healthc. Mater. 5 (2016) 2092–2104.
[84] K. Hayashi, et al., Magnetically responsive smart nanoparticles for Cancer treatment with a combination of magnetic hyperthermia and remote-control drug release, Theranostics 4 (2014) 834–844.
[85] A. Makridis, et al., In vitro application of Mn-ferrite nanoparticles as novel magnetic hyperthermia agents, J. Mater. Chem. B 2 (2014) 8390–8398.
[86] S. Kumar, et al., Theranostic fluorescent silica encapsulated magnetic nanoassemblies for in vitro MRI imaging and hyperthermia, RSC Adv. 5 (2015) 53180–53188.
[87] J. Xie, et al., High-performance PEGylated Mn–Zn ferrite nanocrystals as a passive-targeted agent for magnetically induced cancer theranostics, Biomaterials 35 (2014) 9126–9136.
[88] K. Wu, et al., Functionalized magnetic iron oxide/alginate core-shell nanoparticles for targeting hyperthermia, IJN 3315 (2015), https://doi.org/10.2147/IJN.S68719.
[89] G. Hemery, et al., Monocore *vs.* multicore magnetic iron oxide nanoparticles: uptake by glioblastoma cells and efficiency for magnetic hyperthermia, Mol. Syst. Des. Eng. 2 (2017) 629–639.
[90] M.C. Franchini, et al., In vivo anticancer evaluation of the hyperthermic efficacy of anti-human epidermal growth factor receptor-targeted PEG-based nanocarrier containing magnetic nanoparticles, IJN 3037 (2014), https://doi.org/10.2147/IJN.S61273.
[91] K. Hayashi, et al., Superparamagnetic nanoparticle clusters for Cancer Theranostics combining magnetic resonance imaging and hyperthermia treatment, Theranostics 3 (2013) 366–376.
[92] E. Guisasola, et al., Beyond Traditional Hyperthermia: In Vivo Cancer Treatment with Magnetic-Responsive Mesoporous Silica Nanocarriers, ACS Appl. Mater. Interfaces 10 (2018) 12518–12525.
[93] S. Rana, N.V. Jadhav, K.C. Barick, B.N. Pandey, P.A. Hassan, Polyaniline shell cross-linked Fe_3O_4 magnetic nanoparticles for heat activated killing of cancer cells, Dalton Trans. 43 (2014) 12263–12271.
[94] J. Majeed, et al., Enhanced specific absorption rate in silanol functionalized Fe 3 O 4 core–shell nanoparticles: study of Fe leaching in Fe 3 O 4 and hyperthermia in L929 and HeLa cells, Colloids Surf. B: Biointerfaces 122 (2014) 396–403.
[95] M. Cho, et al., Assembly of Iron oxide Nanocubes for enhanced Cancer hyperthermia and magnetic resonance imaging, Nanomaterials 7 (2017) 72.
[96] S. Mondal, et al., Hydroxyapatite coated Iron oxide nanoparticles: A promising nanomaterial for magnetic hyperthermia Cancer treatment, Nanomaterials 7 (2017) 426.
[97] M.A. Mackey, M.R.K. Ali, L.A. Austin, R.D. Near, M.A. El-Sayed, The Most effective gold Nanorod size for Plasmonic Photothermal therapy: theory and *in vitro* experiments, J. Phys. Chem. B 118 (2014) 1319–1326.
[98] A.V.P. Kumar, et al., Recent advances in nanoparticles mediated photothermal therapy induced tumor regression, Int. J. Pharm. 606 (2021) 120848.
[99] H.S. Han, K.Y. Choi, Advances in nanomaterial-mediated Photothermal Cancer therapies: toward clinical applications, Biomedicines 9 (2021) 305.
[100] A.N. Dosumu, et al., Quantification by luminescence tracking of red emissive gold nanoparticles in cells, JACS Au 1 (2021) 174–186.
[101] A. Doughty, et al., Nanomaterial applications in Photothermal therapy for Cancer, Materials 12 (2019) 779.
[102] D. Jaque, et al., Nanoparticles for photothermal therapies, Nanoscale 6 (2014) 9494–9530.
[103] W. Yang, H. Liang, S. Ma, D. Wang, J. Huang, Gold nanoparticle based photothermal therapy: development and application for effective cancer treatment, Sustain. Mater. Technol. 22 (2019) e00109.
[104] E. Hemmer, A. Benayas, F. Légaré, F. Vetrone, Exploiting the biological windows: current perspectives on fluorescent bioprobes emitting above 1000 nm, Nanoscale Horiz. 1 (2016) 168–184.
[105] G. Hong, A.L. Antaris, H. Dai, Near-infrared fluorophores for biomedical imaging, Nat. Biomed. Eng. 1 (2017) 0010.
[106] S. Wu, H.-J. Butt, Near-infrared photochemistry at interfaces based on upconverting nanoparticles, Phys. Chem. Chem. Phys. 19 (2017) 23585–23596.
[107] E. Hemmer, et al., Upconverting and NIR emitting rare earth based nanostructures for NIR-bioimaging, Nanoscale 5 (2013) 11339.
[108] E. Darrigues, et al., 3D cultures for modeling nanomaterial-based photothermal therapy, Nanoscale Horiz. 5 (2020) 400–430.
[109] S.G. Alamdari, et al., Recent advances in nanoparticle-based photothermal therapy for breast cancer, J. Control. Release 349 (2022) 269–303.
[110] J. Verma, et al., Nanoparticle-mediated cancer cell therapy: basic science to clinical applications, Cancer Metastasis Rev. (2023), https://doi.org/10.1007/s10555-023-10086-2.
[111] M. Norouzi, B. Nazari, D.W. Miller, Electrospun-Based Systems in cancer Therapy, in: Electrospun Materials for Tissue Engineering and Biomedical Applications, Elsevier, 2017, pp. 337–356, https://doi.org/10.1016/B978-0-08-101022-8.00013-2.
[112] W. Bian, et al., Review of functionalized nanomaterials for Photothermal therapy of cancers, ACS Appl. Nano Mater. 4 (2021) 11353–11385.
[113] N.R.S. Sibuyi, et al., Multifunctional gold nanoparticles for improved diagnostic and therapeutic applications: A review, Nanoscale Res. Lett. 16 (2021) 174.
[114] N.S. Abadeer, C.J. Murphy, Recent Progress in Cancer thermal therapy using gold nanoparticles, J. Phys. Chem. C 120 (2016) 4691–4716.
[115] W. Yang, et al., Shape effects of gold nanoparticles in photothermal cancer therapy, Materials Today Sustainability 13 (2021) 100078.
[116] S. Tarantino, A.P. Caricato, R. Rinaldi, C. Capomolla, V. De Matteis, Cancer treatment using different shapes of gold-based nanomaterials in combination with conventional physical techniques, Pharmaceutics 15 (2023) 500.
[117] X. Ye, C. Zheng, J. Chen, Y. Gao, C.B. Murray, Using binary surfactant mixtures to simultaneously improve the dimensional Tunability and Monodispersity in the seeded growth of gold Nanorods, Nano Lett. 13 (2013) 765–771.
[118] P.P.P. Kumar, D.-K. Lim, Photothermal effect of gold nanoparticles as a nanomedicine for diagnosis and therapeutics, Pharmaceutics 15 (2023) 2349.

[119] X. Wang, G. Li, Y. Ding, S. Sun, Understanding the photothermal effect of gold nanostars and nanorods for biomedical applications, RSC Adv. 4 (2014) 30375–30383.
[120] Y. Wang, A.B. Serrano, K. Sentosun, S. Bals, L.M. Liz-Marzán, Stabilization and encapsulation of gold Nanostars mediated by dithiols, Small 11 (2015) 4314–4320.
[121] L. Rodríguez-Lorenzo, J.M. Romo-Herrera, J. Pérez-Juste, R.A. Alvarez-Puebla, L. M. Liz-Marzán, Reshaping and LSPR tuning of au nanostars in the presence of CTAB, J. Mater. Chem. 21 (2011) 11544.
[122] R. Zhou, et al., Gold Nanorods-based Photothermal therapy: interactions between biostructure, nanomaterial, and Near-infrared irradiation, Nanoscale Res. Lett. 17 (2022) 68.
[123] H. Yang, et al., The impact of size and surface ligand of gold nanorods on liver cancer accumulation and photothermal therapy in the second near-infrared window, J. Colloid Interface Sci. 565 (2020) 186–196.
[124] M. Chu, et al., Near-infrared laser light mediated cancer therapy by photothermal effect of Fe3O4 magnetic nanoparticles, Biomaterials 34 (2013) 4078–4088.
[125] J. Zhu, J. Wang, Y. Li, Recent advances in magnetic nanocarriers for tumor treatment, Biomed. Pharmacother. 159 (2023) 114227.
[126] J. Estelrich, M. Busquets, Iron oxide nanoparticles in Photothermal therapy, Molecules 23 (2018) 1567.
[127] T. He, et al., Dual-stimuli-responsive Nanotheranostics for dual-targeting Photothermal-enhanced chemotherapy of tumor, ACS Appl. Mater. Interfaces 13 (2021) 22204–22212.
[128] C. Shirata, et al., Near-infrared photothermal/photodynamic therapy with indocyanine green induces apoptosis of hepatocellular carcinoma cells through oxidative stress, Sci. Rep. 7 (2017) 13958.
[129] A. Neshastehriz, Z. Khosravi, H. Ghaznavi, A. Shakeri-Zadeh, Gold-coated iron oxide nanoparticles trigger apoptosis in the process of thermo-radiotherapy of U87-MG human glioma cells, Radiat. Environ. Biophys. 57 (2018) 405–418.
[130] K. Yang, et al., Graphene in mice: ultrahigh in vivo tumor uptake and efficient Photothermal therapy, Nano Lett. 10 (2010) 3318–3323.
[131] Y. Zhang, C.Y. Ang, Y. Zhao, Polymeric nanocarriers incorporating near-infrared absorbing agents for potent photothermal therapy of cancer, Polym. J. 48 (2016) 589–603.
[132] C. Korupalli, et al., Recent advances of polyaniline-based biomaterials for phototherapeutic treatments of tumors and bacterial infections, Bioengineering 7 (2020) 94.
[133] L. Wang, R. Vivek, W. Wu, G. Wang, J.-Y. Wang, Fabrication of Stable and Well-Dispersed Polyaniline–Polypyrrolidone Nanocomposite for Effective Photothermal Therapy, ACS Biomater Sci. Eng. acsbiomaterials.7b00910 (2018), https://doi.org/10.1021/acsbiomaterials.7b00910.
[134] F. An, et al., Rationally assembled albumin/indocyanine green nanocomplex for enhanced tumor imaging to guide photothermal therapy, J Nanobiotechnol 18 (2020) 49.
[135] S. Mukherjee, L. Liang, O. Veiseh, Recent advancements of magnetic nanomaterials in Cancer therapy, Pharmaceutics 12 (2020) 147.
[136] D.P.N. Gonçalves, et al., Enhanced targeting of invasive glioblastoma cells by peptide-functionalized gold nanorods in hydrogel-based 3D cultures, Acta Biomater. 58 (2017) 12–25.
[137] X. Li, et al., Formation of gold Nanostar-coated hollow mesoporous silica for tumor multimodality imaging and Photothermal therapy, ACS Appl. Mater. Interfaces 9 (2017) 5817–5827.
[138] J. Chen, et al., Indocyanine green-loaded gold nanostars for sensitive SERS imaging and subcellular monitoring of photothermal therapy, Nanoscale 9 (2017) 11888–11901.
[139] B. Gong, et al., Thermo-responsive polymer encapsulated gold nanorods for single continuous wave laser-induced photodynamic/photothermal tumour therapy, J Nanobiotechnol 19 (2021) 41.
[140] J. Liao, K. Shi, Y. Jia, Y. Wu, Z. Qian, Gold nanorods and nanohydroxyapatite hybrid hydrogel for preventing bone tumor recurrence via postoperative photothermal therapy and bone regeneration promotion, Bioactive Materials 6 (2021) 2221–2230.
[141] W. Xu, et al., A dual-targeted hyaluronic acid-gold nanorod platform with triple-stimuli responsiveness for photodynamic/photothermal therapy of breast cancer, Acta Biomater. 83 (2019) 400–413.
[142] Q. You, et al., BSA–bioinspired gadolinium hybrid-functionalized hollow gold Nanoshells for NIRF/PA/CT/MR Quadmodal diagnostic imaging-guided Photothermal/photodynamic Cancer therapy, ACS Appl. Mater. Interfaces 9 (2017) 40017–40030.
[143] L. Zhou, X. Gong, Y. Zhao, J. Xu, Y. Guo, Preparation and characterization of GNRs stabled with the thiolated lemon polysaccharide and the applications for tumor photothermal therapy, Int. J. Biol. Macromol. 224 (2023) 1303–1312.
[144] H.H. Han, et al., Bimetallic hyaluronate-modified au@Pt nanoparticles for noninvasive photoacoustic imaging and Photothermal therapy of skin Cancer, ACS Appl. Mater. Interfaces 15 (2023) 11609–11620.
[145] Y. Yu, et al., Efficacy of Temozolomide-conjugated gold nanoparticle Photothermal therapy of drug-resistant glioblastoma and its mechanism study, Mol. Pharm. 19 (2022) 1219–1229.
[146] N. Zhao, L. Yan, J. Xue, K. Zhang, F.-J. Xu, Degradable one-dimensional dextran-iron oxide nanohybrids for MRI-guided synergistic gene/photothermal/magnetolytic therapy, Nano Today 38 (2021) 101118.
[147] C.C. Barrera, H. Groot, W.L. Vargas, D.M. Narváez, Efficacy and molecular effects of a reduced graphene oxide/Fe_3O_4 nanocomposite in Photothermal therapy against Cancer, IJN 15 (2020) 6421–6432.
[148] A. Kolokithas-Ntoukas, et al., Condensed clustered Iron oxides for ultrahigh Photothermal conversion and *in vivo* multimodal imaging, ACS Appl. Mater. Interfaces 13 (2021) 29247–29256.
[149] X. Zhang, et al., Intracellular pH-propelled assembly of smart carbon nanodots and selective photothermal therapy for cancer cells, Colloids Surf. B: Biointerfaces 188 (2020) 110724.
[150] P. McKernan, et al., Targeted single-walled carbon nanotubes for Photothermal therapy combined with immune checkpoint inhibition for the treatment of metastatic breast Cancer, Nanoscale Res. Lett. 16 (2021) 9.
[151] D.M. Valcourt, M.N. Dang, E.S. Day, IR820-loaded PLGA nanoparticles for photothermal therapy of triple-negative breast cancer, J. Biomed. Mater. Res. 107 (2019) 1702–1712.
[152] K. Mortezaee, et al., Synergic effects of nanoparticles-mediated hyperthermia in radiotherapy/chemotherapy of cancer, Life Sci. 269 (2021) 119020.
[153] X. Wu, J. Liu, L. Yang, F. Wang, Photothermally controlled drug release system with high dose loading for synergistic chemo-photothermal therapy of multidrug resistance cancer, Colloids Surf. B: Biointerfaces 175 (2019) 239–247.
[154] A. Zhang, et al., Synergistic effects of gold Nanocages in hyperthermia and radiotherapy treatment, Nanoscale Res. Lett. 11 (2016) 279.
[155] J.-H. Lee, et al., On-demand drug release system for in vivo Cancer treatment through self-assembled magnetic nanoparticles, Angew. Chem. Int. Ed. 52 (2013) 4384–4388.
[156] Y. Wang, et al., Enhancing targeted Cancer treatment by combining hyperthermia and radiotherapy using Mn–Zn ferrite magnetic nanoparticles, ACS Biomater Sci. Eng. 6 (2020) 3550–3562.
[157] F. Zhang, et al., Magnetic nanoparticles coated with polyphenols for spatio-temporally controlled cancer photothermal/immunotherapy, J. Control. Release 326 (2020) 131–139.
[158] J.G. Mehtala, et al., Synergistic effects of cisplatin chemotherapy and gold nanorod-mediated hyperthermia on ovarian cancer cells and tumors, Nanomedicine 9 (2014) 1939–1955.
[159] R. Wang, et al., PEGylated hollow gold nanoparticles for combined X-ray radiation and photothermal therapy in vitro and enhanced CT imaging in vivo, Nanomedicine 16 (2019) 195–205.
[160] X. Tu, et al., Efficient cancer ablation by combined photothermal and enhanced chemo-therapy based on carbon nanoparticles/doxorubicin@SiO 2 nanocomposites, Carbon 97 (2016) 35–44.
[161] C.A. Robertson, D.H. Evans, H. Abrahamse, Photodynamic therapy (PDT): A short review on cellular mechanisms and cancer research applications for PDT, J. Photochem. Photobiol. B Biol. 96 (2009) 1–8.
[162] E. Ostańska, D. Aebisher, D. Bartusik-Aebisher, The potential of photodynamic therapy in current breast cancer treatment methodologies, Biomed. Pharmacother. 137 (2021) 111302.
[163] C. Kong, X. Chen, Combined photodynamic and Photothermal therapy and immunotherapy for Cancer treatment: A review, IJN 17 (2022) 6427–6446.
[164] W. Zeng, et al., Dual-response oxygen-generating MnO2 nanoparticles with polydopamine modification for combined photothermal-photodynamic therapy, Chem. Eng. J. 389 (2020) 124494.
[165] Pullan Shreffler, Mallik Dailey, Brooks., Overcoming hurdles in nanoparticle clinical translation: the influence of experimental design and surface modification, IJMS 20 (2019) 6056.
[166] P. Zhang, et al., Cancer nanomedicine toward clinical translation: obstacles, opportunities, and future prospects, Med 4 (2023) 147–167.
[167] C. Vilches, R. Quidant, Targeted hyperthermia with plasmonic nanoparticles, in: Frontiers of Nanoscience 16, Elsevier, 2020, pp. 307–352.
[168] A.Q. Figueiredo, et al., Metal-polymer Nanoconjugates application in Cancer imaging and therapy, Nanomaterials 12 (2022) 3166.
[169] C.L. West, A.C.V. Doughty, K. Liu, W.R. Chen, Monitoring tissue temperature during photothermal therapy for cancer, J Bio-X Res 2 (2019) 159–168.
[170] D. Tosi, S. Poeggel, I. Iordachita, E. Schena, Fiber Optic Sensors for Biomedical Applications, in: Opto-Mechanical Fiber Optic Sensors, Elsevier, 2018, pp. 301–333, https://doi.org/10.1016/B978-0-12-803131-5.00011-8.
[171] A. Beccaria, et al., Temperature monitoring of tumor hyperthermal treatments with optical fibers: comparison of distributed and quasi-distributed techniques, Opt. Fiber Technol. 60 (2020) 102340.
[172] A. Nexha, J.J. Carvajal, M.C. Pujol, F. Díaz, M. Aguiló, Lanthanide doped luminescence nanothermometers in the biological windows: strategies and applications, Nanoscale 13 (2021) 7913–7987.
[173] E.F.J. Ring, K. Ammer, Infrared thermal imaging in medicine, Physiol. Meas. 33 (2012) R33–R46.
[174] U. Rocha, et al., Subtissue thermal sensing based on neodymium-doped LaF_3 nanoparticles, ACS Nano 7 (2013) 1188–1199.
[175] B. del Rosal, E. Ximendes, U. Rocha, D. Jaque, In vivo luminescence Nanothermometry: from materials to applications, Advanced Optical Materials 5 (2017) 1600508.
[176] J. Zhou, B. del Rosal, D. Jaque, S. Uchiyama, D. Jin, Advances and challenges for fluorescence nanothermometry, Nat. Methods 17 (2020) 967–980.
[177] C.D.S. Brites, S. Balabhadra, L.D. Carlos, Lanthanide-based thermometers: at the cutting-edge of luminescence thermometry, Advanced Optical Materials 7 (2019) 1801239.
[178] A. Bednarkiewicz, L. Marciniak, L.D. Carlos, D. Jaque, Standardizing luminescence nanothermometry for biomedical applications, Nanoscale 12 (2020) 14405–14421.
[179] M. Quintanilla, L.M. Liz-Marzán, Guiding rules for selecting a Nanothermometer, Nano Today 19 (2018) 126–145.

[180] A. Bednarkiewicz, et al., Luminescence based temperature bio-imaging: status, challenges, and perspectives, Appl. Phys. Rev. 8 (2021) 011317.
[181] J.S. Donner, S.A. Thompson, M.P. Kreuzer, G. Baffou, R. Quidant, Mapping intracellular temperature using green fluorescent protein, Nano Lett. 12 (2012) 2107–2111.
[182] M. Nakano, et al., Genetically encoded ratiometric fluorescent thermometer with wide range and rapid response, PLoS One 12 (2017) e0172344.
[183] H. Zhao, A. Vomiero, F. Rosei, Tailoring the Heterostructure of colloidal quantum dots for Ratiometric optical Nanothermometry, Small 16 (2020) 2000804.
[184] L.J. Mohammed, K.M. Omer, Carbon dots as new generation materials for Nanothermometer: review, Nanoscale Res. Lett. 15 (2020) 182.
[185] S.S. Laha, et al., Nanothermometry measure of muscle efficiency, Nano Lett. 17 (2017) 1262–1268.
[186] A. Nexha, M.C. Pujol Baiges, J.J. Carvajal Martí, Luminescent Nanothermometers Operating Within Biological Windows, in: J.J. Carvajal Martí, M.C. Pujol Baiges (Eds.), Luminescent Thermometry, Springer International Publishing, Cham, 2023, pp. 221–268, https://doi.org/10.1007/978-3-031-28516-5_6.
[187] K. Okabe, et al., Intracellular temperature mapping with a fluorescent polymeric thermometer and fluorescence lifetime imaging microscopy, Nat. Commun. 3 (2012) 705.
[188] S.A. Qureshi, et al., Recent development of fluorescent Nanodiamonds for optical biosensing and disease diagnosis, Biosensors 12 (2022) 1181.
[189] T.F. Segawa, R. Igarashi, Nanoscale quantum sensing with nitrogen-vacancy centers in nanodiamonds – A magnetic resonance perspective, Prog. Nucl. Magn. Reson. Spectrosc. 134–135 (2023) 20–38.
[190] G. Kucsko, et al., Nanometre-scale thermometry in a living cell, Nature 500 (2013) 54–58.
[191] S. Sotoma, H. Okita, S. Chuma, Y. Harada, Quantum nanodiamonds for sensing of biological quantities: angle, temperature, and thermal conductivity, BIOPHYSICS **19**, n/a (2022).
[192] M. Quintanilla, Y. Zhang, L.M. Liz-Marzán, Subtissue Plasmonic Heating Monitored with CaF_2 :Nd^{3+},Y^{3+} Nanothermometers in the Second Biological Window, Chem. Mater. 30 (2018) 2819–2828.
[193] Y. Cui, F. Zhu, B. Chen, G. Qian, Metal–organic frameworks for luminescence thermometry, Chem. Commun. 51 (2015) 7420–7431.
[194] E. Carrasco, et al., Intratumoral thermal Reading during photo-thermal therapy by multifunctional fluorescent nanoparticles, Adv. Funct. Mater. 25 (2015) 615–626.
[195] X. Zhu, et al., Temperature-feedback upconversion nanocomposite for accurate photothermal therapy at facile temperature, Nat. Commun. 7 (2016) 10437.
[196] X. Zhu, et al., Upconversion nanocomposite for programming combination cancer therapy by precise control of microscopic temperature, Nat. Commun. 9 (2018) 2176.
[197] B. del Rosal, et al., Infrared-emitting QDs for thermal therapy with real-time subcutaneous temperature feedback, Adv. Funct. Mater. 26 (2016) 6060–6068.
[198] R. Gupta, D. Sharma, Therapeutic response differences between 2D and 3D tumor models of magnetic hyperthermia, Nanoscale Adv. 3 (2021) 3663–3680.
[199] I. Van Zundert, B. Fortuni, S. Rocha, From 2D to 3D Cancer cell models—the enigmas of drug delivery research, Nanomaterials 10 (2020) 2236.
[200] C. García-Jiménez, C.R. Goding, Starvation and Pseudo-starvation as drivers of Cancer metastasis through translation reprogramming, Cell Metab. 29 (2019) 254–267.
[201] J.M. Ayuso, et al., Tumor-on-a-chip: a microfluidic model to study cell response to environmental gradients, Lab Chip 19 (2019) 3461–3471.
[202] B. Zhang, Y. Hu, Z. Pang, Modulating the tumor microenvironment to enhance tumor nanomedicine delivery, Front. Pharmacol. 8 (2017) 952.
[203] M. Kapałczyńska, et al., 2D and 3D cell cultures – a comparison of different types of cancer cell cultures, aoms (2016), https://doi.org/10.5114/aoms.2016.63743.
[204] R.C. Dutta, A.K. Dutta, 3D Cell Culture: Fundamentals and Applications in Tissue Engineering and Regenerative Medicine, Jenny Stanford Publishing, 2018, https://doi.org/10.1201/b22417.
[205] T.T. Goodman, C.P. Ng, S.H. Pun, 3-D tissue culture Systems for the Evaluation and Optimization of nanoparticle-based drug carriers, Bioconjug. Chem. 19 (2008) 1951–1959.
[206] G. Lazzari, P. Couvreur, S. Mura, Multicellular tumor spheroids: a relevant 3D model for the in vitro preclinical investigation of polymer nanomedicines, Polym. Chem. 8 (2017) 4947–4969.
[207] F. Foglietta, R. Canaparo, G. Muccioli, E. Terreno, L. Serpe, Methodological aspects and pharmacological applications of three-dimensional cancer cell cultures and organoids, Life Sci. 254 (2020) 117784.
[208] K. Kretzschmar, Cancer research using organoid technology, J. Mol. Med. 99 (2021) 501–515.
[209] Z. Li, et al., Application of animal models in Cancer research: recent Progress and future prospects, CMAR 13 (2021) 2455–2475.
[210] R.O. Rodrigues, et al., Organ-on-a-Chip: A preclinical microfluidic platform for the Progress of nanomedicine, Small 16 (2020) 2003517.
[211] E. Lilley, R. Isbrucker, I. Ragan, A. Holmes, Integrating 3Rs approaches in WHO guidelines for the batch release testing of biologicals, Biologicals 74 (2021) 24–27.
[212] G. Perini, et al., Advanced usage of Ti3C2Tx MXenes for photothermal therapy on different 3D breast cancer models, Biomed. Pharmacother. 153 (2022) 113496.
[213] A.M.K. Law, et al., Advancements in 3D cell culture Systems for Personalizing Anti-Cancer Therapies, Front. Oncol. 11 (2021) 782766.
[214] D.T. Leong, K.W. Ng, Probing the relevance of 3D cancer models in nanomedicine research, Adv. Drug Deliv. Rev. 79–80 (2014) 95–106.
[215] S. Kreß, C. Almeria, S. Nebel, D. Faust, C. Kasper, Application of scaffold-free 3D models, in: C. Kasper, D. Egger, A. Lavrentieva (Eds.), Basic Concepts on 3D Cell Culture, Springer International Publishing, Cham, 2021, pp. 147–174, https://doi.org/10.1007/978-3-030-66749-8_7.
[216] S. Gunti, A.T.K. Hoke, K.P. Vu, N.R. London, Organoid and spheroid tumor models: techniques and applications, Cancers 13 (2021) 874.
[217] D. Antoni, H. Burckel, E. Josset, G. Noel, Three-dimensional cell culture: A breakthrough in vivo, IJMS 16 (2015) 5517–5527.
[218] M.A.G. Barbosa, C.P.R. Xavier, R.F. Pereira, V. Petrikaitė, M.H. Vasconcelos, 3D cell culture models as Recapitulators of the tumor microenvironment for the screening of anti-Cancer drugs, Cancers 14 (2021) 190.
[219] R.L.F. Amaral, M. Miranda, P.D. Marcato, K. Swiech, Comparative analysis of 3D bladder tumor spheroids obtained by forced floating and hanging drop methods for drug screening, Front. Physiol. 8 (2017) 605.
[220] S. Nath, G.R. Devi, Three-dimensional culture systems in cancer research: focus on tumor spheroid model, Pharmacol. Ther. 163 (2016) 94–108.
[221] V. Brancato, R.L. Reis, S.C. Kundu, 3D cancer Spheroids and Microtissues, in: Biomaterials for 3D Tumor Modeling 217–234, Elsevier, 2020, https://doi.org/10.1016/B978-0-12-818128-7.00010-1.
[222] M. Zanoni, et al., Modeling neoplastic disease with spheroids and organoids, J. Hematol. Oncol. 13 (2020) 97.
[223] G.A. Busslinger, et al., The potential and challenges of patient-derived organoids in guiding the multimodality treatment of upper gastrointestinal malignancies, Open Biol. 10 (2020) 190274.
[224] D.E. Ingber, Is it time for reviewer 3 to request human organ Chip experiments instead of animal validation studies? Adv. Sci. 7 (2020) 2002030.
[225] M. Russo, C.M. Cejas, G. Pitingolo, Advances in microfluidic 3D cell culture for preclinical drug development, in: Progress in Molecular Biology and Translational Science 187, Elsevier, 2022, pp. 163–204.
[226] N.S. Corsini, J.A. Knoblich, Human organoids: new strategies and methods for analyzing human development and disease, Cell 185 (2022) 2756–2769.
[227] C.M. Leung, et al., A guide to the organ-on-a-chip, Nat Rev Methods Primers 2 (2022) 33.
[228] B. Pinto, A.C. Henriques, P.M.A. Silva, H. Bousbaa, Three-dimensional spheroids as in vitro preclinical models for Cancer research, Pharmaceutics 12 (2020) 1186.
[229] J. Liu, K. Liu, L. Feng, Z. Liu, L. Xu, Comparison of nanomedicine-based chemotherapy, photodynamic therapy and photothermal therapy using reduced graphene oxide for the model system, Biomater. Sci. 5 (2017) 331–340.
[230] B. Crawford, et al., Photothermal ablation of inflammatory breast cancer tumor emboli using plasmonic gold nanostars, IJN 12 (2017) 6259–6272.
[231] H. Li, et al., Molecular bottlebrush as a unimolecular vehicle with tunable shape for photothermal cancer therapy, Biomaterials 178 (2018) 620–629.
[232] D. Kalinowska, et al., Studies on effectiveness of PTT on 3D tumor model under microfluidic conditions using aptamer-modified nanoshells, Biosens. Bioelectron. 126 (2019) 214–221.
[233] J.B. Mamani, et al., Magnetic hyperthermia therapy in glioblastoma tumor on-a-Chip model, Einstein (São Paulo) 18 (2019) eAO4954.
[234] S. Jin, et al., Surface chemistry-mediated penetration and gold nanorod thermotherapy in multicellular tumor spheroids, Nanoscale 5 (2013) 143–146.
[235] C. Roma-Rodrigues, I. Pombo, A.R. Fernandes, P.V. Baptista, Hyperthermia induced by gold nanoparticles and visible light Photothermy combined with chemotherapy to tackle doxorubicin sensitive and resistant colorectal tumor 3D spheroids, IJMS 21 (2020) 8017.
[236] I. Mó, C.G. Alves, D. de Melo-Diogo, R. Lima-Sousa, I.J. Correia, Assessing the combinatorial chemo-Photothermal therapy mediated by Sulfobetaine methacrylate-functionalized nanoparticles in 2D and 3D in vitro Cancer models, Biotechnol. J. 15 (2020) 2000219.
[237] L.P. Ferreira, et al., Screening of dual chemo-photothermal cellular nanotherapies in organotypic breast cancer 3D spheroids, J. Control. Release 331 (2021) 85–102.
[238] P. Bangde, T. Pant, G. Gaikwad, R. Jain, P. Dandekar, Trimethyl chitosan coated palladium nanoparticles as a photothermal agent and its in vitro evaluation in 2D and 3D model of breast cancer cells, Colloids Surf. B: Biointerfaces 211 (2022) 112287.
[239] A.K. Mapanao, M. Santi, V. Voliani, Combined chemo-photothermal treatment of three-dimensional head and neck squamous cell carcinomas by gold nano-architectures, J. Colloid Interface Sci. 582 (2021) 1003–1011.
[240] D. Cassano, et al., Photothermal effect by NIR-responsive excretable ultrasmall-in-nano architectures, Mater. Horiz. 6 (2019) 531–537.
[241] C. Caro, et al., Fe3O4-au Core-Shell nanoparticles as a multimodal platform for in vivo imaging and focused Photothermal therapy, Pharmaceutics 13 (2021) 416.
[242] S.M. Ardekani, et al., Two-photon excitation triggers combined chemo-photothermal therapy via doped carbon nanohybrid dots for effective breast cancer treatment, Chem. Eng. J. 330 (2017) 651–662.
[243] J. Whitney, et al., 3D viability imaging of tumor phantoms treated with single-walled carbon nanohorns and photothermal therapy, Nanotechnology 24 (2013) 275102.
[244] M. Chirivì, et al., Biomimetic keratin-coated gold nanoparticles for photo-thermal therapy in a 3D bioprinted glioblastoma tumor model, IJMS 23 (2022) 9528.
[245] N.A. Stocke, et al., Toxicity evaluation of magnetic hyperthermia induced by remote actuation of magnetic nanoparticles in 3D micrometastasic tumor tissue analogs for triple negative breast cancer, Biomaterials 120 (2017) 115–125.

[246] S. Piehler, et al., Hyperthermia affects collagen fiber architecture and induces apoptosis in pancreatic and fibroblast tumor hetero-spheroids in vitro, Nanomedicine 28 (2020) 102183.
[247] H. Villuendas, C. Vilches, R. Quidant, Standardization of *in vitro* studies for Plasmonic Photothermal therapy, ACS Nanosci. Au 3 (2023) 347–352.
[248] M. Quintanilla, et al., Thermal monitoring during photothermia: hybrid probes for simultaneous plasmonic heating and near-infrared optical nanothermometry, Theranostics 9 (2019) 7298–7312.